R. & M. No. 3806

PROCUREMENT EXECUTIVE, MINISTRY OF DEFENCE

AERONAUTICAL RESEARCH COUNCIL
REPORTS AND MEMORANDA

Measurements of Control-Surface Oscillatory Derivatives on a Sweptback, Tapered Model Wing in two Transonic Tunnels

By N. C. LAMBOURNE, K. C. WIGHT AND B. L. WELSH
Structures Department, R.A.E., Bedford

LONDON: HER MAJESTY'S STATIONERY OFFICE
1977
£5 net

Measurements of Control-Surface Oscillatory Derivatives on a Sweptback, Tapered Model Wing in two Transonic Tunnels

By N. C. LAMBOURNE, K. C. WIGHT AND B. L. WELSH

Structures Department, R.A.E., Bedford

Reports and Memoranda No. 3806*

March, 1976

Summary

Results of measurements of control-surface oscillatory derivatives on a sweptback, tapered half-model of a lifting surface of aspect ratio 2 are presented. The measurements were obtained during the development of a derivative rig which measures normal force, pitching moment, wing bending moment and hinge moment due to control surface oscillation. They were made in the 18 in. × 14 in. (0·46 m × 0·36 m) N.P.L. Teddington tunnel and the 3 ft (0·91 m) R.A.E. Bedford tunnel, the rig being found to operate satisfactorily in both situations. Mach number was varied from 0·4 to 1·0 and stagnation pressure from 0·5 to 2·3 bar. With this combination of Mach number and stagnation pressure, Reynolds number varied from 1 to 6 millions based on mean chord.

The effects of varying the control-surface deflection amplitude from 0·4 to 1·6 degrees and the oscillation frequency from 20 to 70 Hz were examined. The effect of tunnel interference was assessed by measurements in ventilated and closed wall working sections in each tunnel.

Most of the tests were carried out with transition bands on the model, but a few tests were made with the bands removed. The measured derivatives are compared with those obtained by theoretical methods of calculation.

* Replaces R.A.E. Technical Report 76007–A.R.C. 36 716.

LIST OF CONTENTS

1. Introduction

The measurements reported here were primarily undertaken as part of the proving tests of a rig designed to measure the derivatives due to control-surface oscillation. The performance of the rig needed to be assessed in the appropriate wind tunnel situation before deciding on the construction of new models for which measurements are required. For the purpose of testing the rig it was convenient to use an existing model (representative of a wing or tail surface) for which derivative calculations had already been made; thus, as well as providing a test of the equipment, some comparisons between experiment and theory could be made.

Measurements were first made in the 18 in. × 14 in. (0·46 m × 0·36 m) tunnel at Teddington and following satisfactory operation there, further series of measurements were made in the 3 ft (0·91 m) tunnel at Bedford which is the intended location for the future measurements.

The rig is described in Ref. 1. The present Report, apart from demonstrating satisfactory operation of the equipment, gives the results of the measurements, draws conclusions regarding wind tunnel interference and provides comparison between measured and calculated derivatives.

2. Definition of Model and Measured Quantities

The measurements were made on a wall-mounted half-model conforming to planform E of the F and V series[2], the geometrical details of which are given in Fig. 1. A point worthy of note is that the biconvex streamwise sections of the model entail a sharp leading edge which had unfortunate implications when the wing was set at incidence. For convenience the term 'flap' will be used in place of 'control surface'. For the measurement, the flap was forced to oscillate sinusoidally in rotation about its hinge whilst the main portion of the model remained stationary. The aerodynamic hinge moment was extracted from measurement of the torque in the drive shaft, while the principal aerodynamic forces and moments on the combined wing and flap were obtained from measurements with a dynamic balance to which the model was attached. Specifically the balance readings were reduced to yield the wing forces, namely normal force Z, pitching moment M, and bending moment B acting on the complete model in addition to hinge moment H, acting on the flap, as defined by the system of axes shown in the diagram of Fig. 2. In the general oscillatory case each of these quantities is complex consisting of a real part inphase, and an imaginary part inquadrature, with the oscillatory displacement of the flap. For the purpose of this Report it is convenient to call the inphase and inquadrature components the p- and q-components of each complex quantity.

The non-dimensional form of each force and moment is also complex and, as shown in the text of Fig. 2, can be represented in alternative ways: either as a complex derivative (e.g. $\bar{z}_\beta$ consisting of a modulus and phase angle (e.g. $|\bar{z}_\beta|$, ϕ_z), or as p- and q-components (e.g. z_β, $\bar{\nu} z_{\dot{\beta}}$). It should be noted that in the first method of representation it is most convenient for the phase angle to be the phase displacement of the negative of the force or moment coefficient with respect to the flap displacement, because then the lags or leads are always less than $\pi/2$. The second method of representation involves the aerodynamic inphase and inquadrature derivatives (e.g. z_β, $z_{\dot{\beta}}$, h_β and $h_{\dot{\beta}}$). The negative of the real, or inphase, derivative is conventionally termed an aerodynamic stiffness: direct stiffness as for $(-h_\beta)$, or cross stiffness as for $(-z_\beta)$. The negative of the imaginary, or inquadrature, derivative is termed an aerodynamic damping: direct damping as for $(-h_{\dot{\beta}})$, or cross damping as for $(-z_{\dot{\beta}})$.

The above nomenclature assumes a linear situation in which sinusoidal motion of the flap engenders aerodynamic forces that are also pure sinusoids. In reality there is always the possibility that the forces may contain higher harmonics, but in most of the present experiments these components were not found to be significant and the measurements were confined to the fundamental inphase and inquadrature components.

Attention is drawn to the particular manner in which flap deflection and hinge moment are defined in this Report. Following a commonly used convention the flap deflection β refers to an angle measured in a streamwise plane (i.e. a plane normal to the y axis); thus β corresponds to a larger angle $\beta \sec \Delta_h$ measured in a plane normal to the hinge-line, where Δ_h is the hinge-line sweepback. The values of wing force derivative if referred to unit flap angle measured normal to the hinge-line would therefore be smaller (by the factor $\cos \Delta_h$) than the values given herein. Consistent with the above definition of β, the so-called 'hinge moment', H, of this Report is really $\sec \Delta_h \times$ (true moment about hinge). Thus values of hinge-moment derivatives representing true moment per unit flap angle measured normal to the hinge-line would be smaller, by the factor $\cos^2 \Delta_h$, than the hinge-moment derivatives given herein.

3. Model Construction and Measuring System

The geometrical details of the model have already been shown in Fig. 1. The fixed part of the model was constructed of solid steel and its root was rigidly attached to the frame of the dynamic balance. The flap was

hinged to the fixed part of the model by a strip of spring steel and was driven in oscillation by a shaft contained within the thickness of the model and connected to forcing gear outside the tunnel wall. Details of the drive to the flap, the hinge-moment measuring unit and the dynamic balance are described in Ref. 1, whilst the process of extracting the aerodynamic forces and moments is described in Section 6. After an initial series of tests to examine the effects of boundary layer transition, roughness bands were added to upper and lower surfaces of the model. These consisted of tapered areas extending from 10 to 15 per cent of the chord from the leading edge onto which a sparse and random distribution of ballotini was glued. The size of the ballotini (grade 13, approximate diameter 0·11 mm) was chosen to be slightly larger than that calculated by the method of Braslow and Knox[3] for a stagnation pressure of 1 bar.

4. Wind Tunnels

The 18 in. × 14 in. tunnel, the 'smaller' tunnel, was induction-driven and had a stagnation pressure ranging from 1 to 2·5 bar. In the condition in which it was used for the majority of measurements it had a ventilated working section with solid sides and slotted liners at the top and bottom. The internal cross section of this working section was 0·36 m wide by 0·43 m high, the open area ratio of the liners being 9·1 per cent.

The 3 ft tunnel, the 'larger tunnel, is a continuous compressor-driven tunnel with a nominal range of stagnation pressure from 0·25 to 2·0 bar. The majority of measurements in it were made in a ventilated working section (called TABS) 0·91 m wide by 0·67 m high with solid sides and slotted top and bottom liners having an open area ratio of 13·6 per cent. In order to examine the effects of wall interference on the derivatives, some measurements were made in both tunnels with closed (i.e. unventilated) working sections. In the smaller tunnel, the closed wall condition was obtained by sealing the slots with plastic adhesive tape, in which case the cross section remained the same. In the larger tunnel, the closed condition was obtained by removing the top and bottom slotted liners, so that in this case the closed section (0·91 m × 0.91 m) was larger than the ventilated section.

5. Range of Parameters

Table 1 shows the general coverage of parameters.

Mach number was varied from 0·4 to 1·0. Stagnation pressure was varied between 1·0 and 2·3 bar in the 18 in. × 14 in. tunnel and between 0·5 and 1·5 bar in the 3 ft tunnel. Based on mean chord, these variations correspond to approximate ranges of Reynolds number, 2 to 6×10^6 in the smaller tunnel and 1 to 5×10^6 in the larger tunnel. For all the oscillatory tests the mean flap angle was zero; most of the tests were made for an amplitude of 0·8 degrees but in the larger tunnel some measurements were made with additional amplitudes 0·4, 1·2 and 1·6 degrees. In the main tests the wing incidence was zero, but a few measurements were made for incidence 1 and 5 degrees. Oscillatory tests were made for a range of frequency from 20 to 70 Hz and static measurements were made with steady flap deflection to correspond to the zero frequency case. Most of the measurements presented and discussed in the present Report are for a frequency 70 Hz which corresponds to a frequency parameter based on wing mean chord varying approximately from 0·6 to 0·25 as the Mach number varies from 0·4 to 1·0 (see Table 1).

6. Determination of Aerodynamic Forces

The operation of the dynamic balance is fully described in Ref. 1. Briefly, the balance comprises three sets of strain gauge units corresponding in an ideal situation to normal force, pitching moment and bending moment reespectively. However, because of interactions it was necessary to treat the required force and moment components as linear combinations of the outputs from the three strain gauge bridges. Hinge moment was determined directly from the output of a fourth strain gauge bridge incorporated in a torque-measuring unit in the drive shaft of the flap.

The time-varying electrical output from each strain gauge bridge consisted of the force signal in response to the oscillatory motion of the flap together with some amount of random-type noise generated by tunnel flow fluctuations. In some cases, the noise was considerably larger than the signals to be measured. The first step in processing the signals from the force and moment bridges was to feed each in turn, along with a reference signal representing the flap motion, to a transfer function analyser (TFA). In effect the TFA performed a cross correlation of each pair of signals and yielded the required p- and q-components respectively inphase and inquadrature with the flap motion. Each reading of the TFA corresponded to an analysis of 100 cycles of motion; normally all readings were repeated five times and the average was used in the subsequent data reductions. Readings were taken with the tunnel running and in still-air, and the wing forces were then

obtained by the matrix relation:

$$\begin{bmatrix} Z \\ M \\ B \end{bmatrix} = [C](\tilde{E}_v - \tilde{E}_0)$$

where

$\tilde{E}_v$ is a vector of complex amplitudes of the bridge outputs obtained with the tunnel running,

$\tilde{E}_0$ is the corresponding vector measured in still-air,

C is a 3×3 matrix of complex factors obtained by calibration at the appropriate frequency as described in Ref. 1.

The aerodynamic hinge moment was simply obtained by the application of a single complex calibration factor to the difference of wind-on and still-air torque readings.

It is important to note that each aerodynamic force or moment is obtained as the difference between a balance reading with the tunning running and one obtained in still-air. There are two points to be considered regarding this procedure. Firstly, it is only valid when the model is stiff enough for the oscillatory aerodynamic loads to cause only negligible distortion and thus neglible change in the intertial loads appearing at the balance. Secondly, the procedure is, in principle, liable to involve errors due to contributions from the air forces acting in still-air. The inphase and inquadrature balance readings in still-air include contributions from the still-air virtual inertia and the air damping respectively. The former provides a negative inphase contribution, the latter a positive inquadrature one. Simply taking the difference between a wind-on and a still-air reading means that an aerodynamic stiffness so obtained is, if anything too large and an aerodynamic damping too small. A preferable procedure is to obtain balance tare values appropriate to vacuum conditions, but in the present case this was not done. However, past experience of derivative measurements under similar circumstances, but where vacuum tare values have been obtained, indicates that in the present case the involvement of still-air forces should not cause significant error. This is confirmed by the results of measurements made with different tunnel stagnation pressures (to be described in detail in Sections 7.2.3 and 7.2.4). For these measurements the still-air tare readings were all obtained under atmospheric pressure. Since in the present case the non-dimensional value of a stiffness or damping derivative is, in effect, obtained by dividing the difference between wind-on and still-air readings by the stagnation pressure H_0, the non-dimensional measured quantities have the forms:

$$R'_\beta = R_\beta + I/H_0$$

$$R'_{\dot\beta} = R_{\dot\beta} - D/H_0$$

where R_β and $R_{\dot\beta}$ are the true wind-on values,

I and D are constants relating respectively to the virtual inertia and air damping in still-air at atmospheric pressure.

Thus the involvement of quantities I and D could in principle lead to a variation in the *measured* non-dimensional derivatives with stagnation pressure. It is possible for the *true* derivatives to change with stagnation pressure on account of the change of Reynolds number, and there are of course other means through which stagnation pressure might be expected to affect the measurements. However, the fact is that provided boundary layer transition was fixed, the non-dimensional derivatives were found to be independent of stagnation pressure. The implications with regard to the effect of Reynolds number will be discussed in Section 7.2.4; for the moment, this experimental finding is regarded as plausible evidence that negligible errors arise from the still-air virtual inertia and air damping.

7. Results of Measurements

7.1. Accuracy

Before describing the results of the measurements and the influence of various parameters, it is necessary to consider the accuracy of the measured quantities, the relative sizes of the inphase and inquadrature components and the implications that follow about the possible errors in the data presented. At this stage it is useful to refer to a particular set of measurements obtained for $M = 0{\cdot}8$ and frequency 70 Hz ($\bar{\nu} = 0{\cdot}31$) that are tabulated in Fig. 3 as stiffness and damping derivatives and displayed on an Argand diagram as complex quantities. It will be noticed that only the hinge moment has a substantial phase difference with respect to the flap displacement, the phase difference of the other component forces $\bar{z}_\beta$, $\bar{m}_\beta$ and $\bar{b}_\beta$ being not more than a few

degrees. The phase differences are, of course, even smaller when the frequency is reduced. As will be discussed in the later sections, changes in Mach number and various other conditions lead to changes in both the magnitude and phase of the forces. Those encountered in the present tests involved changes of magnitude but never the sign of the inphase components. But in some cases the inquadrature components changed both in magnitude and sign. The smallness of the phase angles has a large effect on the percentage accuracy of the cross damping derivatives $z_{\dot\beta}$. $m_{\dot\beta}$ and $b_{\dot\beta}$ as will now be discussed.

Although the oscillatory forces and moments were measured as p- and q-components and the results are presented mostly in the form of stiffness and damping derivative coefficients, it is more convenient to relate accuracy to the precison of measuring the amplitude and phase of the electrical signals corresponding to the forces. If we suppose there is a possible error of $\pm n$ per cent in the measurement of an amplitude A, and a possible error of $\pm\varepsilon$ rad in the measurement of a phase ϕ, the possible errors in the p- and q-components are approximately

$$\pm A[(n/100)\cos\phi + \varepsilon \sin|\phi|] \text{ in the } p\text{-component, } A\cos\phi$$

$$\pm A[(n/100)\sin|\phi| + \varepsilon\cos\phi] \text{ in the } q\text{-component, } A\sin\phi.$$

Information about accuracy comes from two sources: firstly, an analysis of the possible magnitude of random errors using the results of a series of repeat measurements; secondly, a consideration of possible systematic errors bases on our subjective assessments regarding the measuring equipment and its calibration. With regard to the former, an examination of repeatability in the 3 ft tunnel for flap amplitude 0·8 degrees and frequency 70 Hz was made by taking ten, instead of the usual five repeated readings. The results suggest that in general for the usual five repeated readings, the standard error of the mean* is:

wing forces, Z, M and B, $\pm 1{\cdot}5$ per cent in amplitude $\pm 0{\cdot}75$ degrees in phase angle
hinge-moment H, $\pm 0{\cdot}5$ per cent in amplitude $\pm 0{\cdot}75$ in phase angle.

Since these values are the result of experiment, they take into account all random errors arising in the measuring system due, for instance, to fluctuations in the wind tunnel flow, variations in oscillation amplitudes and the effect of signal noise generally.

With regard to an assessment of possible systematic errors, a general and necessarily subjective consideration of the instruments used suggests a possible error of 1·5 per cent in the measurement of signal amplitude and a possible error of about 1 degree in phase which are therefore slightly in excess of the random errors. Thus putting $n = 1{\cdot}5$ and $\varepsilon = 0{\cdot}015$ (a convenient substitute for $1/57{\cdot}3$) in the expression for the errors in the p- and q-components, we arrive at the simplified expression

$$\pm 0{\cdot}015A[\cos\phi + \sin|\phi|]$$

for the possible error in either. For the derivatives, the p- and q-components of hinge-moments are h_β and $\bar\nu h_{\dot\beta}$ respectively, so that the possible error in each is

$$\pm 0{\cdot}015|\bar h_\beta|[\cos\phi_h + \sin|\phi_h|]$$

where

$$|\bar h_\beta|^2 = h_\beta^2 + (\bar\nu h_{\dot\beta})^2 \text{ and } \tan\phi_h = \bar\nu h_{\dot\beta}/h_\beta.$$

Similar expressions relate to the other force and moment derivatives.

For oscillation at 70 Hz, the phase angle of the hinge moment lies between 18 and 40 degrees depending on Mach number, so that the possible percentage error in h_β is approximately 2 or 3 per cent and that in $h_{\dot\beta}$ between 3 and 6 per cent. For a lower frequency, the proportional error in $h_{\dot\beta}$ would be larger because of the decrease in phase angle. For the normal force, pitching moment and bending moment, the phase angles are sufficiently small for the possible errors to be approximately $\pm 0{\cdot}015\,A$ for both p- and q-components. Furthermore, because ϕ is small for the wing forces, the amplitude A is little different from the magnitude of the p-component, so that whilst the possible error in a cross stiffness derivative is ± 1.5 per cent, the errors in the cross damping derivatives for frequency 70 Hz, based on a mean value of $\bar\nu$, are of order:

$$\pm 0{\cdot}05\begin{pmatrix} z_b \\ m_\beta \\ b_\beta \end{pmatrix} \quad \text{in} \quad \begin{pmatrix} z_{\dot\beta} \\ m_{\dot\beta} \\ b_{\dot\beta} \end{pmatrix}.$$

* Standard error of the mean $= \sigma/\sqrt{N}$ where, σ = standard deviation, N = number of observations.

For measurements made at the frequency 20 Hz, the possible errors in the damping derivatives are approximately 3.5 times larger.

Most of the graphical presentation of results include an indication of accuracy based on these assessments.

7.2 Influence of Parameters

7.2.1. *Mach number.* The manner in which the derivative coefficients change with Mach number is essentially the same in the two tunnels. Results obtained in the larger tunnel are shown in Figs. 4 to 7 and show similar trends for the extreme oscillation frequencies 20 Hz and 70 Hz. The coefficients of the cross stiffnesses, i.e. z_β, m_β and b_β, remain fairly constant with increasing Mach number until $M = 0{\cdot}85$ above which their magnitudes decrease as the sonic condition is approached. This decrease seems to herald the large reduction in control effectiveness which would occur if the Mach number were raised sufficiently for the local flow over the model to become completely supersonic; in which case, deflection of the control would have little influence on the flow over the fixed part of the model. The cross-dampings, i.e. $z_{\dot\beta}$, $m_{\dot\beta}$ and $b_{\dot\beta}$ vary in an almost linear manner with Mach number, including a change of sign. Each wing force leads the flap motion at low Mach number and lags at the higher Mach numbers. For the normal force the change of sign occurs just above $M = 0{\cdot}4$, but for pitching moment and bending moment the change occurs at approximately $M = 0{\cdot}7$. For $M = 0{\cdot}9$, the respective lag angles are approximately

$$-\phi_z = \tan^{-1}(0{\cdot}30\,\bar{\nu}), \qquad -\phi_m = \tan^{-1}(0{\cdot}11\,\bar{\nu}) \quad \text{and} \quad -\phi_b = \tan^{-1}(0{\cdot}14\,\bar{\nu}).$$

The magnitude of the hinge-moment stiffness derivative shows a reduction with increasing Mach number which is similar for the two frequencies. The lead of hinge moment on flap motion varies from $\tan^{-1}(0{\cdot}7\,\bar{\nu})$ at $M = 0{\cdot}4$ to $\tan^{-1}(1{\cdot}7\,\bar{\nu})$ at $M = 0{\cdot}9$, with a further large increase to $\tan^{-1}(3{\cdot}3\,\bar{\nu})$ at $M = 1{\cdot}0$. No lagging hinge moment which would correspond to negative damping was encountered at any of the test conditions and frequencies.

7.2.2. *Oscillation frequency.* The differences between the derivatives for 20 Hz and 70 Hz can be seen in the previously mentioned diagrams, Figs. 4 to 7. Results for the other test frequencies fall between these two sets. Furthermore steady derivatives obtained by displacing the control surface by a known angle and measuring the steady outputs from the strain gauge units showed only small differences from the inphase derivatives for 20 Hz.

Because of the lack of any large effect of frequency, only the results for 70 Hz (since these provide the greatest accuracy for the damping derivatives) will be used in discussing the effects of other parameters.

7.2.3. *Transition fixing.* At an early stage in the measurements in the smaller tunnel some unexplained day-to-day variations in repeated measurements indicated a sensitivity to small changes in tunnel flow and suggested the need for an investigation into the desirability of fixing boundary layer transition. The initial tests with the roughness bands, already described in Section 3, were made with a stagnation pressure of 1 bar. Before roughness bands were applied, an oil-film examination of the surface flow at zero incidence with the flap stationary was inconclusive with regard to boundary layer transition. But when the model was set at 1 degree incidence, the oil patterns showed a separation bubble on the upper surface close behind the leading edge, presumably caused by the flow detaching at the sharp leading edge. On the lower surface the oil patterns showed a laminar boundary layer extending over an appreciable area of the wing; for $M = 0.6$ it extended some 75 mm from the leading edge and thus up to the flap hinge over the outboard region. When a roughness band was attached to the lower surface only, the transition position moved forward. Measurements at $M = 0{\cdot}8$ showed that this roughness band caused reductions of the order of 10 to 20 per cent in the magnitudes of each of the Z, M and H oscillatory forces. For 1 degree incidence application of a roughness band to the upper surface in addition to the one on the lower surface produced hardly any further change in the forces. This evidence showed that the oscillatory forces were sensitive to the nature of the boundary layer. Whereas the boundary layer on the upper surface was already turbulent due to the leading edge separation, that on the lower surface was changed by the application of roughness, and this in turn apparently affected the oscillatory forces.

In the absence of roughness bands the magnitudes of the forces, although not always repeatable, were greater at zero incidence than at 1 degree. For both incidences the magnitudes were reduced by roughness bands and the value of the forces for the two incidences were then in good agreement.

The effects of attaching roughness band were further examined when the stagnation pressure was increased to 1·8 bar. Except for the hinge-moment damping all the oscillatory forces were less affected by transition fixing at the higher stagnation pressure than they were at the lower stagnation pressure. With transition fixed,

the forces were the same for the two stagnation pressures (*see* also Section 7.2.4). Fig. 8 shows the results for the hinge-moment derivatives including the exceptional result for $h_{\dot{\beta}}$ where transition fixing has a greater effect at the higher stagnation pressure. The general reduction in the magnitude of the hinge-moment derivatives due to transition fixing is in agreement with the conclusion of Moore[4].

From a consideration of all the evidence of our tests on the effects of roughness, it seems probable that for the Reynolds numbers of the tests, and with the sharp leading edge of the model, the transition position for the zero incidence would be sensitive to small changes of flow angle at the leading edge unless roughness bands were present. Thus it seems possible that, in the absence of roughness bands, oscillation of the flap could lead to an oscillation in the transition position and therefore cyclic changes in the boundary layer characteristics which in turn could bring into play additional cyclic aerodynamic forces.

Based on these considerations and the fact that day-to-day variations in the derivatives were thereby eliminated, it was decided to retain the roughness bands for the main body of measurements. However, the discrepancies between theory and experiment, to be discussed later in Section 9, and the appreciable reduction in the derivatives found by the addition of transition bands, which is possibly due to an increase in boundary layer thickness certainly suggest the need for research into viscous effects.

7.2.4. *Reynolds number.* The variation of a derivative with tunnel stagnation pressure can be ascribed to Reynolds number only provided there are not significant changes from other causes (e.g. model distortion, and possibly tunnel turbulence) that are influenced by stagnation pressure. However, it is plausible to regard an insensitivity to changes in stagnation pressure as evidence of an insensitivity to Reynolds number at least over the range covered. As already noted in Section 7.2.3, changing the stagnation pressure from 1·0 to 1·8 bar in the smaller tunnel produced little change in any of the derivatives provided transition was fixed, the results for hinge moment being shown in Fig. 8. A few further measurements at $M = 0{\cdot}6$ in which the stagnation pressure was increased to 2.3 bar also showed no other change in the derivatives. These results coupled with an estimated absence of any significant distortion from the change in aerodynamic loading leads to the conclusion that, provided transition is fixed, the derivatives are not sensitive to Reynolds numbers within the range covered (i.e. $2{\cdot}5 < 10^{-6}\ Re < 4{\cdot}8$ for $M = 0{\cdot}6$). This is in agreement with the general conclusions of Moore based on a survey of previous information on hinge-moment derivatives. To a large extent the conclusion is confirmed by the subsequent measurements in the larger tunnel which show no significant effect of stagnation pressure on any of the derivatives except hinge stiffness, h_{β}. In Fig. 9 this derivative shows little change between 1·0 and 1·4 bar, but an increase in magnitude when stagnation pressure is reduced to 0·5 bar. That is, in the larger tunnel the only significant effect of stagnation pressure appears at the lowest stagnation pressure for which there are no comparative results from the smaller tunnel. Bearing in mind the sensitivity of the derivatives to boundary layer characteristics as described in Section 7.2.3, it seems likely that the change found in the larger tunnel at low stagnation pressure is due to a deficiency in transition fixing. Subsequent calculations of the size of ballotini that would be required to fix transition for 0·5 bar substantiate this view. Unlike the tests in the smaller tunnel, no oil-film examination of the effectiveness of the roughness bands was made in the larger tunnel.

7.2.5. *Oscillation amplitude.* Measurements for flap amplitudes ranging from 0·4 to 1·6 degrees show no large differences in the wing cross-stiffness derivatives. Fig. 10 shows results for z_{β} and $z_{\dot{\beta}}$ which are typical of the amplitude effects on the other wing derivatives. Larger amplitude effects were found on the hinge-moment derivatives, and these effects were dependent on oscillation frequency. The carpet plots of Figs. 11 and 12 show for 70 Hz an almost linear increase in $-h_{\beta}$ with amplitude and a smaller and less consistent change in $h_{\dot{\beta}}$. For both h_{β} and $h_{\dot{\beta}}$, the amplitude effects are greatest for the highest Mach number. Results obtained at a frequency of 20 Hz show less consistent variations and larger amplitude effects at the high Mach numbers including a sharp fall in stiffness and damping for the largest amplitudes, 1·6 degrees at $M = 1.0$. These low stiffness and damping values are given in Table 2 which gives values of h_{β} and $h_{\dot{\beta}}$ for the various amplitudes at $M = 1{\cdot}0$.

7.2.6. *Wing incidence.* Most of the measurements were made for zero incidence but a few measurements covering a range of Mach number and oscillation frequency were made to examine the effects of incidence. One such series of measurements was made with incidence increased to 1 degree, and another with incidence increased to 5 degrees. These showed that, provided the wing was fitted with a transition band, the change of incidence from 0 to 1 degree made no significant difference in any of the derivatives, but the change to 5 degrees produced large alterations in all the derivatives, some stiffness derivatives increasing as much as 25 per cent and some cross dampings changing sign. It is likely that these effects are associated with a substantial flow change occurring between 1 and 5 degrees. The sharp leading edge is known to cause a small separation bubble

even at 1 degree. It seems probable that by 5 degrees the bubble will have changed to a fully developed leading-edge vortex which could modify the flow over the more outboard region of the wing. Although no detailed explanation can be advanced, it seems plausible that the development of this vortex flow would affect the lift effectiveness and hinge moment properties of the flap.

7.3. Tunnel interference

Comparison of measurements made in the 18 in. × 14 in. tunnel and 3 ft tunnel is valuable in assessing the effects of tunnel wall interference. The main measurements in each tunnel were obtained with ventilated top and bottom walls and solid sidewalls. For both tunnels, further measurements were made with all four walls of the working section unventilated (see Section 4 for details). For this condition the maximum speed was restricted to $M = 0{\cdot}8$ in the smaller tunnel and to $M = 0{\cdot}85$ in the larger tunnel.

To provide direct comparisons, measurements in the two tunnels were made for the same oscillation frequency, 70 Hz, and the same stagnation pressure, 1 bar. For the restricted range of Mach numbers we thus have comparisons for four different conditions (two tunnels × two wall conditions) whilst for the higher Mach number we have comparisons between the two tunnels for only the ventilated conditions. Solid blockage corrections to the free stream velocity and Mach number are negligible even for the smaller unventilated tunnel. Although the thicknesses of the sidewall boundary layer were different in the two tunnels, the effect on the derivatives is likely to be small since the aerodynamic loading due to control surface movement is concentrated mainly over the outboard part of the wing. Thus any observed difference in the measured derivatives are considered to be due to differences in 'lift effect' interference.

The results for the eight derivatives over the full range of Mach number are shown in Figs. 13 to 16. The diagrams show comparisons of the four tunnel conditions up to $M \doteq 0{\cdot}8$ and compare the results from the two ventilated working sections up to $M = 0{\cdot}9$. Broadly, the overall agreement between the various tunnel conditions is reassuring, for not only was there a considerable difference in the size of the two tunnels, but the noise level in the larger ventilated tunnel was several times that encountered in the smaller tunnel (*see* Ref. 1). Apart from the differences for the normal force derivatives z_β, $z_{\dot\beta}$ there are no obviously significant differences between the results for the various tunnel conditions and the small discrepancies in the other derivatives do not seem to form a consistent pattern. Even the differences in $z_{\dot\beta}$ assume less significance when compared with the effects of flap amplitude (see Fig. 10).

Below about $M = 0{\cdot}85$, each derivative varies smoothly with Mach number so that it is possible to make the comparison of the four tunnel conditions for a single Mach number. For this purpose $M = 0{\cdot}781$ was chosen because for this Mach number, theoretical interference corrections are available. For each of the four tunnel wall conditions the values of the derivatives measured at $M = 0{\cdot}6$, $0{\cdot}7$ and $0{\cdot}8$ were then used to provide an interpolated value for $M = 0{\cdot}781$. Fig. 17 shows the four values of each complex derivative plotted on an Argand diagram. For each derivative, except bending moment, there is a spread of points which is greater than the estimated possible errors of measurement. The widest spread occurs for the normal force $\bar{z}_\beta$ and for this force component the spread in the moduli follows a pattern consistent with our general knowledge of steady lift-interference. That is, for the smaller tunnel the modulus for the unventilated condition is greater than that for the ventilated condition. There is little difference between the two moduli from the larger tunnel and these lie between those for the smaller tunnel. A tempting interpretation is that each of the values from the larger tunnel is approximately interference-free and the divergence of the values from the smaller tunnel reflect the interference effects of opposite sign for open and closed working sections. It is difficult to discern any consistent pattern in the results for the other derivatives.

The Appendix describes the correction of the measured derivatives for wall interference using a method based on Ref. 5. Fig. 18 shows the values obtained after applying the corrections to the derivatives shown in Fig. 17. There is indeed a dramatic collapse of the dispersion of $\bar{z}_\beta$ and some smaller reductions in the spread of the other derivatives except for $\bar{b}_\beta$. The general conclusion is that for $M \leqslant 0{\cdot}8$ the derivatives that have been obtained in the larger tunnel (i.e. Bedford 3 ft tunnel) are sufficiently close to free-stream values without the need for correction, and that for any of the two wall conditions in the smaller tunnel, the free-stream values could be deduced from the measurements to an accuracy of a few per cent in modulus and a few degrees in phase.

Returning to Figs. 13 and 16 and the comparison between the two ventilated tunnels, we see that at least up to $M = 0{\cdot}9$ the general trends with Mach number show reasonable agreement between the two tunnels. In the light of the discussion of the comparisons for $M \leqslant 0{\cdot}8$, it is reasonable to consider that the larger tunnel gives values closest to free-stream values.

The model-to-tunnel size ratios relevant to wall interference are given in Table 3. In relation to normal wind tunnel practice, the model was somewhat too large for the smaller tunnel but smaller than is usual for the larger tunnel. It is therefore perhaps not surprising to find an absence of significant interference effects in the larger tunnel, at least up to $M = 0{\cdot}85$. For the smaller tunnel, although appreciable effects would certainly be expected for wing motion damping derivatives, it appears that the effects for a part-span control surface are not very important.

8. Preferred Set of Measured Derivatives

The general agreement between the measurements made under various tunnel conditions is considered to be very satisfactory. On the basis that the interference must be less in the larger tunnel we consider the measurements obtained in the slotted 3 ft tunnel with frequency 70 Hz provide the 'best' set of derivatives. The values of the stiffness and damping derivatives together with the moduli and phase angles deduced from the measurements are given in Table 4 together with the estimated accuracy associated with each quantity.

It is interesting to consider the planform position at which the resultant oscillatory lift (i.e. normal force) due to the control surface acts. In general, this oscillatory force acts at a point which is not constant during the cycle of oscillation. If its centre of action is distant $(-X)$ behind the pitching moment axis and distant (Y) measured normal from the root (see Fig. 2), then at times when the flap has maximum displacement,

$$-X/\bar{c} = m_\beta/z_\beta$$

$$y/s = 2b_\beta/z_\beta.$$

This position, known as the centre of action of the inphase lift, which has been deduced in this way from the measurements, is shown in Fig. 19 for the various test Mach numbers. There is only little change in the position between $M = 0{\cdot}4$ and $M = 0.6$, but with further increase of free-stream Mach number up to $M = 1.0$, the centre moves outboard and rearwards. This trend is consistent with the reduction in upstream influence implicit in subsonic compressible flow theory and, on physical grounds, it would be expected when local regions of supersonic flow develop. Theory also predicts that for a small steady deflection of the flap, the centre of action would approach the centroid of the control surface as the free-stream Mach number continues to increase supersonically. It is to be expected that the centre for the inphase lift would behave similarly. As will be seen in Fig. 19, the measured centres of action up to the highest test Mach number, $M = 1{\cdot}0$, certainly appear to be approaching the centroid. Theoretical predictions regarding the centre of action for subsonic speeds will be considered in the following Section.

9. Comparison with Theory

Derivatives for the model planform have been calculated by two methods based on subsonic lifting surface theory, but neither of these methods takes account of wing thickness or boundary layer effects. Before the measurements were made Garner and Lehrian[6], using their low-frequency method, made calculations for a 'tapered swept wing' identical to the present planform. The Z, M, B and H derivatives were calculated for a single Mach number, namely 0·781. Subsequently the zero-frequency inquadrature derivatives were modified on the basis of equation (121) of Ref. 6 to take account of the frequency parameter of the experiment. In Table 5 the zero-frequency inphase derivatives, the modified inquadrature derivatives and the corresponding moduli and phases derived from this source are denoted by G.

After the measurements, Davies, using the method described in Ref. 7, calculated the Z, M and H derivatives for $M = 0{\cdot}6$, 0·781 and 0·927 for values of the frequency parameter appropriate to the experimental values. These derivatives are denoted by D in Tables 5 and 6.

For the purpose of providing an experimental set of derivatives for comparison, the preferred set of measurements (Section 8) has been used to interpolate values of derivatives for the particular Mach numbers of the calculations for which tests were not made. The comparisons extend over the inphase and inquadrature components and their moduli and phases, Table 5 relating to $M = 0.781$ and Table 6 to $M = 0.6$ and 0·927. For each measured quantity the probable bound to the measurement error is indicated. It will be noted that most of the measured cross damping derivatives have no more than one-figure accuracy.

For $M = 0{\cdot}6$ and 0·927, the experimental values have not been corrected for tunnel interference, but the errors on this account are believed to be small apart perhaps from those in the derivative $z_{\dot{\beta}}$. For $M = 0{\cdot}781$ the uncorrected measurements and the values corrected by the method of the Appendix are given. Graphical comparisons are afforded by Figs. 20 to 25 which show the experimental and the theoretical D values plotted against Mach number, and by Figs. 26 to 28 which show, in the form of Argand diagrams the complex

derivative for each of the three Mach numbers. Before commenting on the comparisons we note from the theoretical values of Table 5 that the two methods of calculations are sufficient agreement for us to make general comparisons between 'theory' and experiment.

An outstanding feature of the comparisons, concerns the moduli of the derivatives; the experimental moduli are considerably smaller than the theoretical ones. For both normal force and pitching moment, the ratio of measured to calculated moduli is approximately 0·76 for $M = 0{\cdot}6$ and 0·64 for $M = 0{\cdot}927$. For the hinge moment the ratio is even smaller, being about 0·56 for $M = 0{\cdot}6$ and 0·29 for $M = 0{\cdot}927$. For the hinge moment, the measured phase angles are significantly greater than the calculated ones. In other words, for hinge moment, the disparity between measured and calculated stiffness derivatives is greater than the disparity between the damping derivatives. For instance, for $M = 0{\cdot}6$, the measured hinge-moment stiffness is only 0·56 of the calculated value whilst the measured damping is 0·73 of the calculated value.

The positions of the centre of action of the inphase normal force deduced from the measurements as described in Section 8, are compared in Table 7 with those obtained from theory for $M = 0{\cdot}6, 0{\cdot}782$ and 0·927. Although theory overestimates the magnitudes of the forces, the point of action is reasonably well predicted.

It is interesting to review briefly other comparisons between measured values and the results of inviscid thin-wing theory for an oscillating control surface in subsonic flow. Information exists for two- and three-dimensional wings and is in the form either of direct measurements of hinge moment, or of measurements of chordwise distributions of unsteady pressure, which in some cases have been integrated to provide total forces[8–13]. Apart from one exception[13], the comparisons generally show the measured oscillatory hinge moment is less than the calculated one, and in some cases the modulus and the inphase components are considerably less. For instance, early work by one of the present authors[8] showed that for a two-dimensional system in low speed flow the ratio of measured to calculated hinge moment was approximately 0·6 for both stiffness and damping derivatives. A more recent investigation by Hertrich[11] using a three-dimensional model leads to a rather similar conclusion regarding hinge moment. With regard to wing forces, the integration of the unsteady pressures measured by Hertrich[11] gives a total lift due to the control surface that is only some 75 or 80 per cent of theory. In short, the differences between experiment and theory that have been found in the present tests are reasonably consistent with the results of several previous investigations. Essentially, the differences between experiment and theory are thought to be associated with the omission from the theory of boundary layer and wing thickness effects, which are considered to reinforce each other in the particular case of hinge moment.

In Ref. 6 Garner and Lehrian put forward an empirical method of correcting the calculated damping derivatives to take account of the realistic flow features not included in the theory. The correction is obtained from the experimental value of the corresponding stiffness derivative and the application of equation (124) of Ref. 6. By this means the theoretical damping derivatives for $M = 0{\cdot}781$ have been corrected and these are shown in comparison with the original theoretical values and the experimental values in Table 8. It will be seen that the correction provides a very real improvement as far as hinge-moment damping is concerned, whilst the effect on the wing cross dampings is less dramatic but in each case improves the comparison with experiment.

10. Performance of Measuring Rig

The derivative measuring rig has been used successfully in two tunnels of widely different character, and the results obtained are considered to be of high accuracy. Because of the plans to use the Bedford 3 ft tunnel for further oscillatory control surface measurements, it is particularly gratifying to record that satisfactory performance of the rig has been achieved in that tunnel in spite of the high level of signal-noise from fluctuations in the tunnel flow.

11. Summary of Conclusions

(1) The control-surface oscillatory derivative rig has operated satisfactorily under a variety of conditions in two tunnels. Its performance in the Bedford 3 ft tunnel augurs well for a further programme of measurements that is planned for that tunnel.

(2) Although the test model was small in comparison with the size of the 3 ft tunnel, the evidence concerning the interference effects encountered in the two tunnels suggests that, even with normal sized models where only a control surface is oscillated, no large interference effects will be present in the 3 ft tunnel, at least up to $M = 0{\cdot}9$.

(3) The anomalous and inconsistent changes in the derivatives that occurred when boundary layer transition was not fixed or when the model was at incidence were thought to be due to the sharp leading edge

and its ability to cause flow separation. The measured changes provide a clear indication of the sensitivity of control surface derivatives to viscous effects.

(4) Provided transition was fixed, the measured derivatives were not sensitive to changes of Reynolds number over the range $2{\cdot}0 < Re \times 10^{-6} < 6{\cdot}0$ based on mean chord.

(5) For the particular model used, the measured derivatives most representative of full-scale Reynolds number are considered to be those obtained with fixed transiton. These derivatives have magnitudes appreciably less than those deduced from theory, but the centre of action of the oscillatory lift is in good agreement with theory.

LIST OF SYMBOLS

WING GEOMETRY (See Fig. 1)

x, y, z	Co-ordinate axes
c_r	Wing root chord
$\bar{c}$	Wing mean chord
$\bar{c}_F$	Flap mean chord
s	Wing span
s_F	Flap span
S	Wing area
S_F	Flap area
Λ_h	Hinge-line sweepback

FORCE AND MOMENTS (See Fig. 2 for definitions)

Z	Normal force
M	Pitching moment
B	Bending moment
H	Hinge moment
$z_\beta, m_\beta, b_\beta, h_\beta$, etc. $\phi_z, \phi_m, \phi_b, \phi_h$	Non-dimensional quantities associated with $Z\,M\,B\,H$

FLAP MOTION

β	Angular deflection (radians, unless otherwise stated)
β_1	Amplitude
f	Oscillation frequency (Hz)
$\omega \equiv 2\pi f$	Circular frequency
$\bar{\nu} \equiv \omega\bar{c}/V$	Frequency parameter

GENERAL

M	Mach number
Re	Reynolds number
V	Air velocity
ρ	Air density
$R\{x\}$	Real part of x
p-component	Inphase, or real, component
q-component	Inquadrature, or imaginary component.

REFERENCES

No.	*Author(s)*	*Title, etc.*
1	K. C. Wight and N. C. Lambourne ..	A control-surface oscillatory derivative rig for use with half-models in high speed wing tunnels. A.R.C. C.P. No. 1353 (1975)
2	D. L. Woodcock	Co-ordinated experimental and theoretical research on the oscillatory airforces for selected planforms at subsonic and supersonic speeds. A.R.C. R. & M. 3581 (1968)
3	A. L. Braslow and E. C. Knox	Simplified method for determination of critical height of distributed roughness particles for boundary-layer transition at Mach numbers from 0 to 5. N.A.C.A. T.N. 4363 (1958)
4	A. W. Moore	Scale effects on oscillating control surface derivatives. A.R.C. C.P. No. 1151 (1971)
5	H. C. Garner, A. W. Moore and K. C. Wight	The theory of interference effects on dynamic measurements in slotted-wall tunnels at subsonic speeds and comparisons with experiment A.R.C. R. & M. 3500 (1968)
6	H. C. Garner and Doris E. Lehrian	The theoretical treatment of slowly oscillating part-span control surfaces in subsonic flow A.R.C. R. & M. 3676 (1968)
7	D. E. Davies	Calculation of unsteady generalised airforces on a thin wing oscillating harmonically in subsonic flow A.R.C. R. & M. 3409 (1963)
8	K. C. Wight	Measurements of two-dimensional derivatives on a wing-aileron-tab system with a 1541 section aerofoil. Part I. Direct aileron derivatives A.R.C. R. & M. 2934 (1955) Part II. Direct tab and cross-aileron-tab derivatives A.R.C. R. & M. 3029 (1958)
9	J. B. Bratt, C. J. W. Miles and R. F. Johnson	Measurements of the direct hinge-moment derivatives at subsonic and transonic speeds for a cropped delta wing with oscillating flap. A.R.C. R. & M. 3163 (1957)
10	J. A. Wyss and R. M. Sorenson	An investigation of the control surface flutter derivatives of a N.A.C.A. 65-213 airfoil in the Ames 16 foot high speed wind tunnel N.A.C.A. R.M. A51J10 (1951)

No.	Author(s)	Title, etc.
11	H. Hertrich	Zur experimentellen Prüfung instationärer dreidimensionaler Tragflächentheorien bei incompressibler Strömung. A.V.A. Göttingen Mitteilung 40 (1967) (Experimental verification of unsteady, three-dimensional wing theories in incompressible flow. M.O.D. Translation D.R.I.C.-B.R.-33607, D.I.-11 Trans 1-6422)
12	H. Tijdeman and P. Schippers	Results of pressure measurements on an airfoil with oscillating flap in two-dimensional high subsonic and transonic flow. N.L.R. T.R. 73078U (1973)
13	R. Gray and D. E. Davies	Comparison of experimentally and theoretically determined values of oscillatory aerodynamic control surface hinge moment coefficients. R.A.E. Technical Report 72023 (1972)
14	H. C. Garner	Theoretical use of variable porosity in slotted tunnels for minimising wall interference on dynamic measurements. A.R.C. R. & M. 3706 (1972)
15	H. C. Garner	Numerical appraisal of Multhopp's low-frequency subsonic lifting-surface theory. A.R.C. R. & M. 3634 (1968)

APPENDIX

Approximate Corrections for Wall Interference
By H. C. GARNER

Additional Notation

b	Breadth of tunnel
C	Cross-sectional area of tunnel
F	Slot parameter (see Ref. 14)
h	Height of tunnel
$\bar{w}_i$	Complex interference upwash (see Ref. 5)
x_0	Location of pitching axis
β	Compressibility factor $(1-M^2)^{1/2}$
δ_0, δ_1	Steady lift interference parameters (see Ref. 5)
δ_0'	Inquadrature interference parameter (see Ref. 5)
σ	Span ratio $2s/b$
z_q, m_q, b_q, h_q	Non-dimensional forces associated with angular rate of pitch q ($Z = \rho V S \bar{c} q z_q$, etc.)
$z_\theta, m_\theta, b_\theta, h_\theta$ $z_{\dot\theta}, m_{\dot\theta}, b_{\dot\theta}, h_{\dot\theta}$	Non-dimensional quantities associated with Z, M, B, H for pitching oscillation $\theta = \theta_1 R\{e^{i\omega t}\}$ (definitions as in Fig. 2 with β_1 replaced by θ_1)
subscript T	Denotes uncorrected 'tunnel" value
prefix Δ	Denotes incremental correction for wall interference.

No great precision in evaluating tunnel-wall interference on the present experiments is possible for two reasons. The load distribution due to the oscillation of the part-span control surface is not available; nor is the porosity term in equation (10) of Ref. 14 for the boundary condition at the slotted roof and floor of either of the tunnels. Fortunately the interference corrections are fairly small, so that an approximate procedure based on Refs. 5 and 14 is shown to suffice.

Following the analysis in Section 3 of Ref. 5 for a small model oscillating at low frequency in a subsonic stream, we first replace the complex interference upwash in equation (44) of Ref. 5 by:

$$\frac{\bar{w}_i(x)}{V} = \frac{2\beta_1 S}{C}\Big[-\delta_0 z_{\beta T} + \frac{\delta_1 \bar{c}}{\beta h}\Big(m_{\beta T} - \frac{x-x_0}{\bar{c}} z_{\beta T}\Big) + \\ + i\bar{\nu}\Big\{-\frac{\delta_0' h}{\beta \bar{c}} z_{\beta T} + \delta_0\Big(-z_{\dot\beta T} - m_{\beta T} + \frac{x-x_0}{\bar{c}} z_{\beta T}\Big) + \\ + \frac{\delta_1 \bar{c}}{\beta h}\Big(m_{\dot\beta T} - \frac{x-x_o}{\bar{c}} z_{\dot\beta T}\Big)\Big\}\Big], \tag{A-1}$$

without the final quadratic term in x. Thus equation (49) and (50) of Ref. 5 are replaced by incremental corrections

$$\Delta z_\beta = -\frac{2S}{C}\Big[\Big(-\delta_0 z_{\beta T} + \frac{\delta_1 \bar{c}}{\beta h} m_{\beta T}\Big) z_\theta - \frac{\delta_1 \bar{c}}{\beta h} z_{\beta T} z_q\Big] \tag{A-2}$$

and

$$\Delta z_{\dot\beta} = -\frac{2S}{C}\Big[\Big(-\delta_0 z_{\dot\beta T} + \frac{\delta_1 \bar{c}}{\beta h} m_{\dot\beta T}\Big) z_\theta - \frac{\delta_1 \bar{c}}{\beta h} z_{\dot\beta T} z_q - \\ - \frac{\delta_0' h}{\beta \bar{c}} z_{\beta T} z_\theta + \delta_0\Big\{-z_{\beta T}(z_{\dot\theta} - 2z_q) - m_{\beta T} z_\theta\Big\}\Big], \tag{A-3}$$

to the measured lift derivatives $z_{\beta T}$ and $z_{\dot\beta T}$. The corresponding corrections Δm_β and $\Delta m_{\dot\beta}$ to the pitching-moment derivatives $m_{\beta T}$ and $m_{\dot\beta T}$ are obtained by substituting $m_\theta, m_q, m_{\dot\theta}$ for $z_\theta, z_q, z_{\dot\theta}$ on the right-hand sides of equations (A-2) and (A-3). The corrections to the bending-moment and hinge-moment derivatives

are obtained similarly; to illustrate, the increments

$$\Delta h_\beta = -\frac{2S}{C}\left[\left(-\delta_0 z_{\beta T} + \frac{\delta_1 \bar{c}}{\beta h} m_{\beta T}\right) h_\theta - \frac{\delta_1 \bar{c}}{\beta h} z_{\beta T} h_q\right] \tag{A-4}$$

and

$$\Delta h_{\dot\beta} = -\frac{2S}{C}\left[\left(-\delta_0 z_{\dot\beta T} + \frac{\delta_1 \bar{c}}{\beta h} m_{\dot\beta T}\right) h_\theta - \frac{\delta_1 \bar{c}}{\beta h} z_{\dot\beta T} h_q - \right.$$
$$\left. - \frac{\delta_0' h}{\beta \bar{c}} z_{\beta T} h_\theta + \delta_0 \left\{ -z_{\beta T}(h_{\dot\theta} - 2h_q) - m_{\beta T} h_\theta \right\} \right], \tag{A-5}$$

are not explicitly dependent on the uncorrected wind-tunnel values $h_{\beta T}$ and $h_{\dot\beta T}$.

To apply these corrections, it is necessary to estimate the various derivatives due to both oscillatory and rotary pitching motion. With the aid of Table 16 of Ref. 6 and Table 39 of Ref. 15 and some further calculations with four chordwise terms ($N = 4$), we obtain the following theoretical values for $M = 0{\cdot}781$ ($\beta = 0{\cdot}625$) and a pitching axis $x_0 = 0{\cdot}808\bar{c}$ through the root mid-chord.

$$\left.\begin{array}{lll} -z_\theta = 1{\cdot}276 & -z_q = 1{\cdot}039 & -z_{\dot\theta} = 1{\cdot}285 \\ -m_\theta = 0{\cdot}349 & -m_q = 0{\cdot}569 & -m_{\dot\theta} = 0{\cdot}769 \\ -b_\theta = 0{\cdot}275 & -b_q = 0{\cdot}242 & -b_{\dot\theta} = 0{\cdot}258 \\ -h_\theta = 0{\cdot}087 & -h_q = 0{\cdot}227 & -h_{\dot\theta} = 0{\cdot}410 \end{array}\right\} \tag{A-6}$$

Of these derivatives the set for hinge moment is least representative of practice, but equations (A-4) and (A-5) yield such small corrections that the uncertainty is of little consequence.

The following geometrical data have been used for the three test configurations.

Tunnel	Roof and floor	$\frac{b}{h}$	F	$\sigma = \frac{2S}{b}$	$\frac{\bar{c}}{n}$	$\frac{S}{C}$
0·46 m × 0·36 m	Slotted	1·657	0·0935	0·5306	0·440	0·233
0·91 m × 0·67 m	Slotted	2·727	0·2692	0·2063	0·281	0·058
0·91 m × 0·91 m	Solid	2·000	—	0·2063	0·206	0·043

In the usual notation of Fig. 1 of Ref. 14 for half-model testing the tunnel breadth b is taken as twice that of the actual tunnel. The slot parameter F has been calculated from equation (5) of Ref. 14.

The procedure in Section 3.2 of Ref. 14 has been used to obtain the following values of the interference parameters δ_0, δ_1 and δ_0'.

Tunnel	Roof and floor	σ	δ_0	δ_1	δ_0'
0·46 m × 0·36 m	Slots sealed	0	0·1228	0·253	−0·0089
		0·5306	0·1050	0·216	−0·0076
	Open	0	−0·2167	−0.316	0·1315
	Open	0·5306	−0·182	−0·265	0·1105
	Ideal slots	0·5306	−0·152	−0·214	0·0980
	Real slots	0·5306	−0·062	−0·064	0·061
0·91 m × 0·91 m	Solid liners	0	0·1368	0·293	−0·0040
		0·2063	0·1286	0·275	−0·0037
0·91 m × 0·67 m	Open	0	−0·3570	−0·522	0·2170
	Open	0·2063	−0·3327	−0·486	0·2022
	Slots sealed	0	0·1793	0·392	−0·0006
	Slots sealed	0·2063	0·1586	0·347	−0·0006
	Ideal slots	0·2063	−0·2095	−0·277	0·1514
	Real slots	0·2063	−0·081	−0·059	0·098

Allowance for span ratio σ rests entirely on equation (38) of Ref. 14 in which δ_0 is deduced under conditions of elliptic spanwise loading, albeit a poor representation of that due to the part-span control. The interference parameters for 'real slots' are from linear interpolations of the form

$$(\delta)_{\text{real slots}} = 0{\cdot}65(\delta)_{\text{ideal slots}} + 0{\cdot}35(\delta)_{\text{slots sealed}} \tag{A-7}$$

in an attempt to allow for the unknown porosity term in the wall boundary condition. The only justification for this is the limited evidence for the 0·46 m × 0·36 m (18 in. × 14 in.) tunnel in Fig. 34 of Ref. 5. Equation (A)7) is also used for the 0·91 m × 0·67 m tunnel in the absence of aerodynamic data concerning the effect of the gauze between the slots and the plenum chamber.

The largest wall corrections occur with the 0·46 m × 0·36 m tunnel, where the corrected values of the derivatives in the following table for $M = 0{\cdot}781$ and $f = 70$ Hz are much more consistent than the uncorrected ones.

Derivative	Uncorrected values		Corrected values	
	Slots sealed	Slots open	Slots sealed	Slots open
$-z_\beta$	0·219	0·199	0·206	0·206
$-z_{\dot\beta}$	−0·075	−0·042	−0·066	−0·069
$-m_\beta$	0·183	0·177	0·175	0·180
$-m_{\dot\beta}$	−0·022	0·000	−0·022	−0·008
$-b_\beta$	0·065	0·064	0·062	0·066
$-b_{\dot\beta}$	−0·007	0·002	−0·004	−0·004
$-h_\beta$	0·132	0·127	0·129	0·129
$-h_{\dot\beta}$	0·144	0·144	0·146	0·142

In the corresponding calculations for the larger tunnel, only $-z_{\dot\beta}$, $-m_{\dot\beta}$ and $-b_{\dot\beta}$ involve corrections of magnitude greater than 0·002, which is no larger than the possible experimental error as indicated in Table 4.

TABLE 1

Range of Parameters

Mach number (nominal)	0·4, 0·6, 0·7, 0·8, 0·85, 0·9, 1·0
Stagnation pressure	0·5 to 2·3 bar
Reynolds number	1 to 6×10^6 (based on mean chord)
Incidence	0, 1, 5°
Control surface amplitude	0·4, 0·8, 1·2, 1·6°
Frequency of oscillation	0, 20, 40, 55, 70 Hz
Transition bands	with or without

Values of Reduced Frequency, $\bar{\nu} \equiv \omega\bar{c}/V$

Frequency Hz	Mach number						
	0·40	0·60	0·70	0·80	0·85	0·90	1·00
20	0·18	0·12	0·10	0·09	0·08	0·08	0·07
70	0·62	0·41	0·35	0·31	0·29	0·28	0·25

TABLE 2

Variation of Hinge Moment Derivatives with Control Surface Amplitude for $M = 1{\cdot}0$

β_1 (deg)	20 Hz, $\bar{\nu}=0{\cdot}07$		70 Hz, $\bar{\nu}=0{\cdot}25$	
	$-h_\beta$	$-h_{\dot\beta}$	$-h_\beta$	$-h_{\dot\beta}$
0·8	0·052	0·257	0·071	0·235
1·2	0·069	0·236	0·091	0·222
1·6	0·016	0·080	0·106	0·222

TABLE 3

Tunnel Interference Parameters

Tunnel	$\frac{\text{Model span}}{\text{Tunnel width}}$ (σ)	$\frac{\text{Model chord}}{\text{Tunnel height}}$ $\frac{\bar{c}}{h}$	$\frac{\text{Model area}}{\text{Tunnel area}}$ $\frac{S}{C}$
18 in. × 14 in. 'smaller'			
ventilated	0·530	0·440	0·233
closed-wall	0·530	0·440	0·233
3 ft 'larger'			
ventilated	0·206	0·281	0·058
closed-wall	0·206	0·206	0·043

TABLE 4

Preferred Set of Measured Derivatives 70 Hz, 3 ft Slotted Tunnel

M	0·40	0·60	0·70	0·80	0·85	0·90	1·00	Possible error
$\bar{\nu}$	0·62	0·41	0·35	0·31	0·29	0·28	0·25	
$-z_\beta$	0·210	0·210	0·209	0·208	0·202	0·199	0·151	±0·003
$-z_{\dot\beta}$	0·011	−0·013	−0·027	−0·040	−0·046	−0·059	−0·070	±0·007
$\lvert\bar{z}_\beta\rvert$	0·210	0·210	0·209	0·208	0·202	0·200	0·152	±0·003
ϕ_z (deg)	1·9	−1·4	−2·6	−3.4	−3·8	−4.7	−6·6	±0·8
$-m_\beta$	0·171	0·170	0·174	0·178	0·176	0·177	0·144	±0·003
$-m_{\dot\beta}$	0·021	0·007	0·002	−0·004	−0·010	−0·019	−0·035	±0·006
$\lvert\bar{m}_\beta\rvert$	0·171	0·170	0·174	0·178	0·176	0·177	0·144	±0·003
ϕ_m (deg)	4·4	1·0	0·2	−0·4	−0·9	−1·7	−3·5	±0·8
$-b_\beta$	0·064	0·065	0·065	0·064	0·065	0·063	0·050	±0·001
$-b_{\dot\beta}$	0·008	0·005	0·000	−0·005	−0·007	−0·009	−0·010	±0·002
$\lvert\bar{b}_\beta\rvert$	0·064	0·065	0·065	0·064	0·065	0·063	0·050	±0·001
ϕ_b (deg)	4·4	1·8	0·0	−1·4	−1·8	−2·3	−2·9	±0·8
$-h_\beta$	0·158	0·152	0·147	0·137	0·127	0·113	0·071	±2%
$-h_{\dot\beta}$	0·112	0·126	0·140	0·154	0·175	0·188	0·235	±5%
$\lvert\bar{h}_\beta\rvert$	0·173	0·161	0·155	0·145	0·137	0·125	0·092	±2%
ϕ_h (deg)	23·7	18·8	18·4	19·2	21·8	25·0	39·6	±0·8

TABLE 5

Comparison of Theory and Experiment

	$M = 0.781$				
	Experiment $\bar{\nu} = 0·32$			Theory	
	Uncorrected	Corrected for w/t interference	Possible error	D (Ref.7) $\bar{\nu} = 0·326$	G (Ref. 6) $\bar{\nu} = 0·31$
$-z_\beta$	0·208	0·210	±0·003	0·293	0·298
$-z_{\dot\beta}$	−0·037	−0·054	±0·007	−0·042	−0·041
$\lvert\bar{z}_\beta\rvert$	0·208	0·211	±0·003	0·293	0·299
ϕ_z (deg)	−3·1	−4·4	±0·8	−2·4	−2·4
$-m_\beta$	0·177	0·178	±0·003	0·244	0·244
$-m_{\dot\beta}$	−0·003	−0·010	±0·006	0·0195	0·020
$\lvert\bar{m}_\beta\rvert$	0·177	0·178	±0·003	0·244	0·245
ϕ_m (deg)	−0·3	−1.0	±0·8	1.4	1·5
$-b_\beta$	0·064	0·064	±0·001	—	0·092
$-b_{\dot\beta}$	−0·004	−0·008	±0·002	—	−0·003
$\lvert\bar{b}_\beta\rvert$	0·064	0·064	±0·001	—	0·092
ϕ_b (deg)	−1.1	−2·1	±0·8	—	−0·5
$-h_\beta$	0·140	0·140	±0·003	0·292	0·303
$-h_{\dot\beta}$	0·151	0·150	±0·006	0·208	0·200
$\lvert\bar{h}_\beta\rvert$	0·147	0·147	±0·003	0·299	0·309
ϕ_h (deg)	17·9	17·8	±0·8	12·0	11·6

TABLE 6

Comparison of Theory and Experiment

	$M = 0{\cdot}6$		$M = 0{\cdot}927$	
	Experimental $\bar{\nu} = 0{\cdot}41$	Theory D $\bar{\nu} = 0{\cdot}414$	Experimental $\bar{\nu} = 0{\cdot}27$	Theory D $\bar{\nu} = 0{\cdot}280$
$-z_\beta$	$0{\cdot}210 \pm 0{\cdot}003$	0·276	$0{\cdot}193 \pm 0{\cdot}003$	0·300
$-z_{\dot{\beta}}$	$-0{\cdot}013 \pm 0{\cdot}007$	0·005	$-0{\cdot}058 \pm 0{\cdot}006$	−0·164
$\lvert\bar{z}_\beta\rvert$	$0{\cdot}210 \pm 0{\cdot}003$	0·276	$0{\cdot}194 \pm 0{\cdot}003$	0·304
ϕ_z (deg)	$-1{\cdot}4 \quad \pm 0{\cdot}8$	0·4	$-5{\cdot}2 \quad \pm 0{\cdot}8$	−9·3
$-m_\beta$	$0{\cdot}170 \pm 0{\cdot}003$	0·222	$0{\cdot}174 \pm 0{\cdot}003$	0·276
$-m_{\dot{\beta}}$	$0{\cdot}007 \pm 0{\cdot}006$	0·036	$-0{\cdot}024 \pm 0{\cdot}006$	−0·063
$\lvert\bar{m}_\beta\rvert$	$0{\cdot}170 \pm 0{\cdot}003$	0·222	$0{\cdot}174 \pm 0{\cdot}003$	0·276
ϕ_m (deg)	$1{\cdot}0 \quad \pm 0{\cdot}8$	3·7	$-2{\cdot}4 \quad \pm 0{\cdot}8$	−3.9
$-b_\beta$	$0{\cdot}065 \pm 0{\cdot}001$	—	$0{\cdot}061 \pm 0{\cdot}001$	—
$-b_{\dot{\beta}}$	$0{\cdot}005 \pm 0{\cdot}002$	—	$-0{\cdot}010 \pm 0{\cdot}002$	—
$\lvert\bar{b}_\beta\rvert$	$0{\cdot}065 \pm 0{\cdot}001$	—	$0{\cdot}061 \pm 0{\cdot}001$	—
ϕ_b (deg)	$1{\cdot}8 \quad \pm 0{\cdot}8$	—	$-2{\cdot}8 \quad \pm 0{\cdot}8$	—
$-h_\beta$	$0{\cdot}152 \pm 0{\cdot}004$	0·271	$0{\cdot}103 \pm 0{\cdot}002$	0·358
$-h_{\dot{\beta}}$	$0{\cdot}126 \pm 0{\cdot}005$	0·170	$0{\cdot}200 \pm 0{\cdot}008$	0·284
$\lvert\bar{h}_\beta\rvert$	$0{\cdot}161 \pm 0{\cdot}004$	0·280	$0{\cdot}119 \pm 0{\cdot}002$	0·368
ϕ_h (deg)	$18{\cdot}2 \quad \pm 0{\cdot}8$	14.1	$30{\cdot}2 \quad \pm 0{\cdot}8$	13·4

TABLE 7

Centre of Action on Inphase Lift

	$M = 0{\cdot}600$		$M = 0{\cdot}781$		$M = 0{\cdot}927$	
	Experiment	Theory	Experiment	Theory	Experiment	Theory
$-X/\bar{c}$	0·81	0·80	0·85	0·82	0·90	0·925
$Y/\bar{c}$	0·62	—	0·62	0·62	0·63	—

TABLE 8

Damping Derivatives for $M = 0{\cdot}781$

Comparison of Theory and Measurement

Derivative	Theory	Theory with empirical correction	Measured	Measured corrected for tunnel interference
$-z_{\dot{\beta}}$	−0·041	−0·054	−0·037 (±0·007)	−0·054 (±0·007)
$-m_{\dot{\beta}}$	+0·020	+0·010	−0·003 (±0·006)	−0·010 (±0·006)
$-b_{\dot{\beta}}$	−0·003	−0·007	−0·004 (±0·002)	−0·008 (±0·002)
$-h_{\dot{\beta}}$	+0·200	+0·145	+0·157 (±0·006)	+0·150 (±0·006)

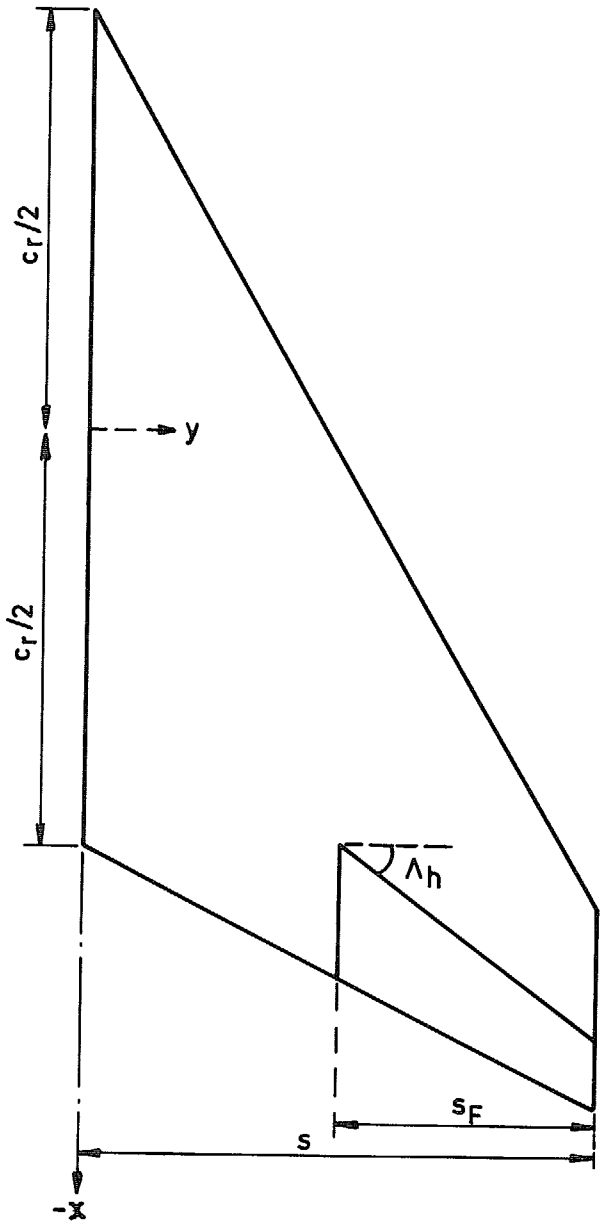

Wing

Streamwise section:
circular arc biconvex
thickness to chord ratio, 0·05

Aspect ratio	2	
Taper ratio	0·238	
Leading edge sweepback	60°	
Trailing edge sweepback	26·57°	
Root chord c_r	304·8 mm	[12 in]
Mean chord $\bar{c}$	188·7 mm	
Semi-span s	188·7 mm	

Control Surface (Flap)

Hinge line sweepback λ_h	36·87°	
Chord ratio	inboard end 0·25 outboard end 0·325	
Span	$s_F = 0{\cdot}5s$	94·35 mm
Mean chord	$\bar{c}_F$	35·36 mm

FIG. 1. Wing planform and control surface details.

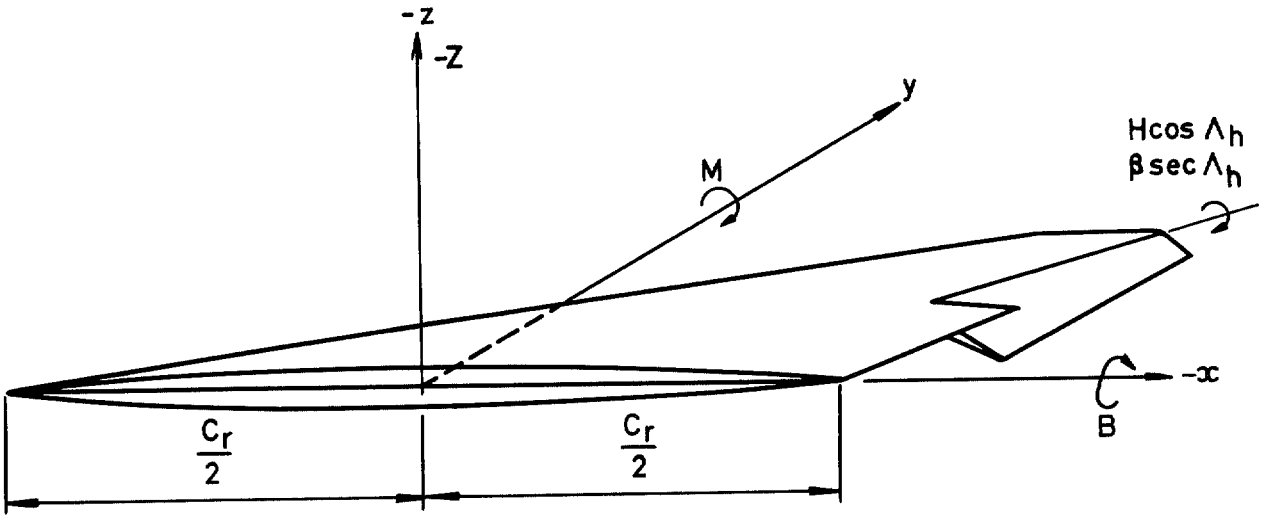

Motion	β	$= \beta_1 R\{e^{i\omega t}\}$
Normal force	Z	$= \rho V^2 S \beta_1 R\{\bar{z}_\beta e^{i\omega t}\}$
Pitching moment	M	$= \rho V^2 S \bar{c} \beta_1 R\{\bar{m}_\beta e^{i\omega t}\}$
Bending moment	B	$= 2\rho V^2 S s \beta_1 R\{\bar{b}_\beta e^{i\omega t}\}$
Flap "hinge moment"	H	$= \rho V^2 S_F \bar{c}_F \beta_1 R\{\bar{h}_\beta e^{i\omega t}\}$
Frequency parameter	$\bar{\upsilon}$	$= \omega \bar{c}/V$

Moduli and phases

$$-\bar{z}_\beta = \{|\bar{z}_\beta|, \phi_z\}$$
$$-\bar{m}_\beta = \{|\bar{m}_\beta|, \phi_m\}$$
$$-\bar{b}_\beta = \{|\bar{b}_\beta|, \phi_b\}$$
$$-\bar{h}_\beta = \{|\bar{h}_\beta|, \phi_h\}$$

p and q components

$$\bar{z}_\beta = z_\beta + i\bar{\upsilon} z_{\dot{\beta}}$$
$$\bar{m}_\beta = m_\beta + i\bar{\upsilon} m_{\dot{\beta}}$$
$$\bar{b}_\beta = b_\beta + i\bar{\upsilon} b_{\dot{\beta}}$$
$$\bar{h}_\beta = h_\beta + i\bar{\upsilon} h_{\dot{\beta}}$$

Stiffness derivatives

$$-z_\beta \, , \; -m_\beta$$
$$-b_\beta \, , \; -h_\beta$$

Damping derivatives

$$-z_{\dot{\beta}} \, , \; -m_{\dot{\beta}}$$
$$-b_{\dot{\beta}} \, , \; -h_{\dot{\beta}}$$

FIG. 2. Definition of axes and oscillatory quantities.

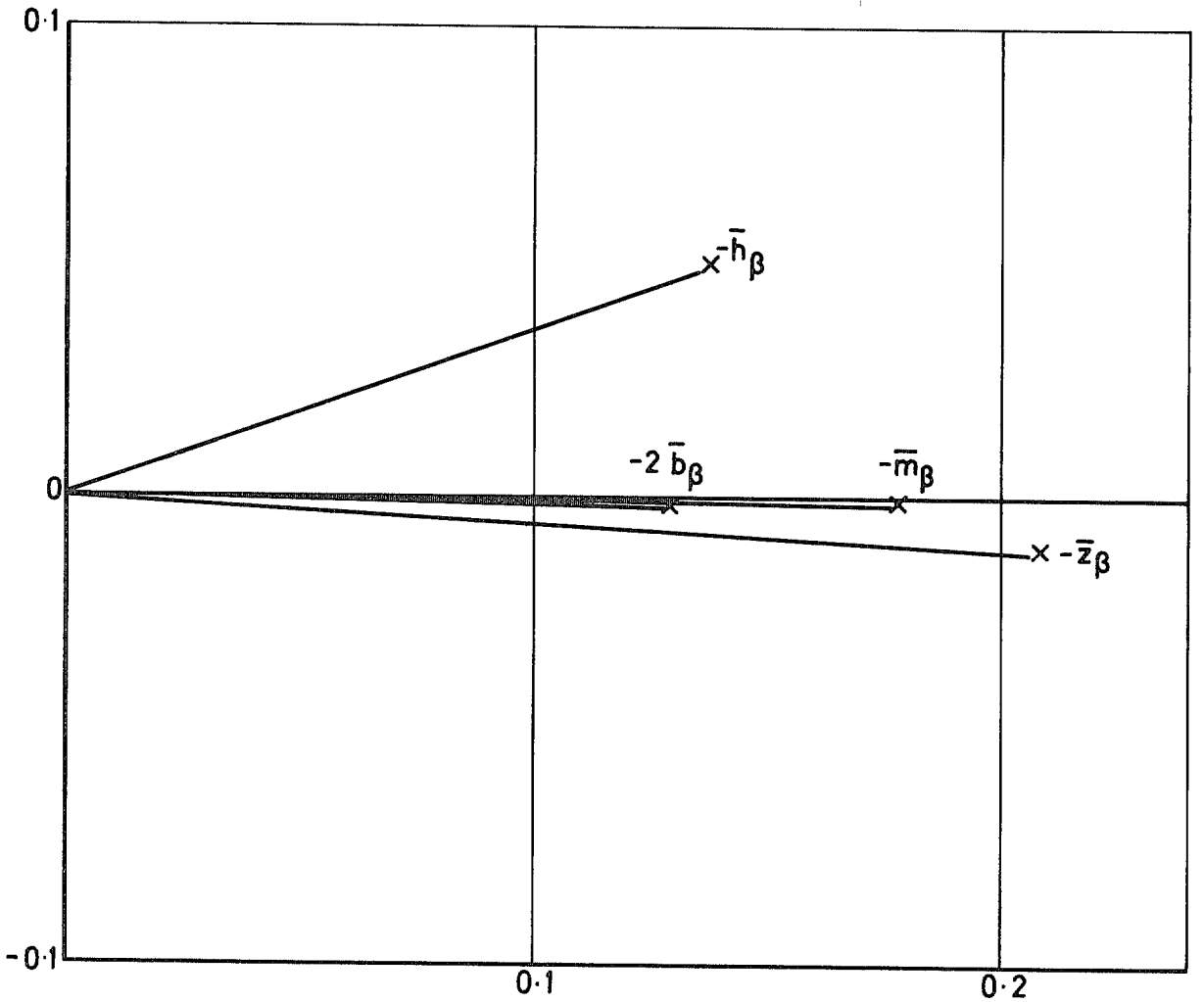

$\bar{z}_\beta = z_\beta + i\bar{v}z_{\dot{\beta}}$; $-z_\beta = 0{\cdot}208$ $-z_{\dot{\beta}} = -0{\cdot}040$

$\bar{m}_\beta = m_\beta + i\bar{v}z_{\dot{\beta}}$; $-m_\beta = 0{\cdot}178$ $-m_{\dot{\beta}} = -0{\cdot}004$

$\bar{b}_\beta = b_\beta + i\bar{v}b_{\dot{\beta}}$; $-b_\beta = 0{\cdot}064$ $-b_{\dot{\beta}} = -0{\cdot}005$

$\bar{h}_\beta = h_\beta + i\bar{v}h_{\dot{\beta}}$; $-h_\beta = 0{\cdot}137$ $-h_{\dot{\beta}} = +0{\cdot}154$

$M = 0{\cdot}8$ $\bar{v} = 0{\cdot}31$

FIG. 3. Typical set of measured derivatives.

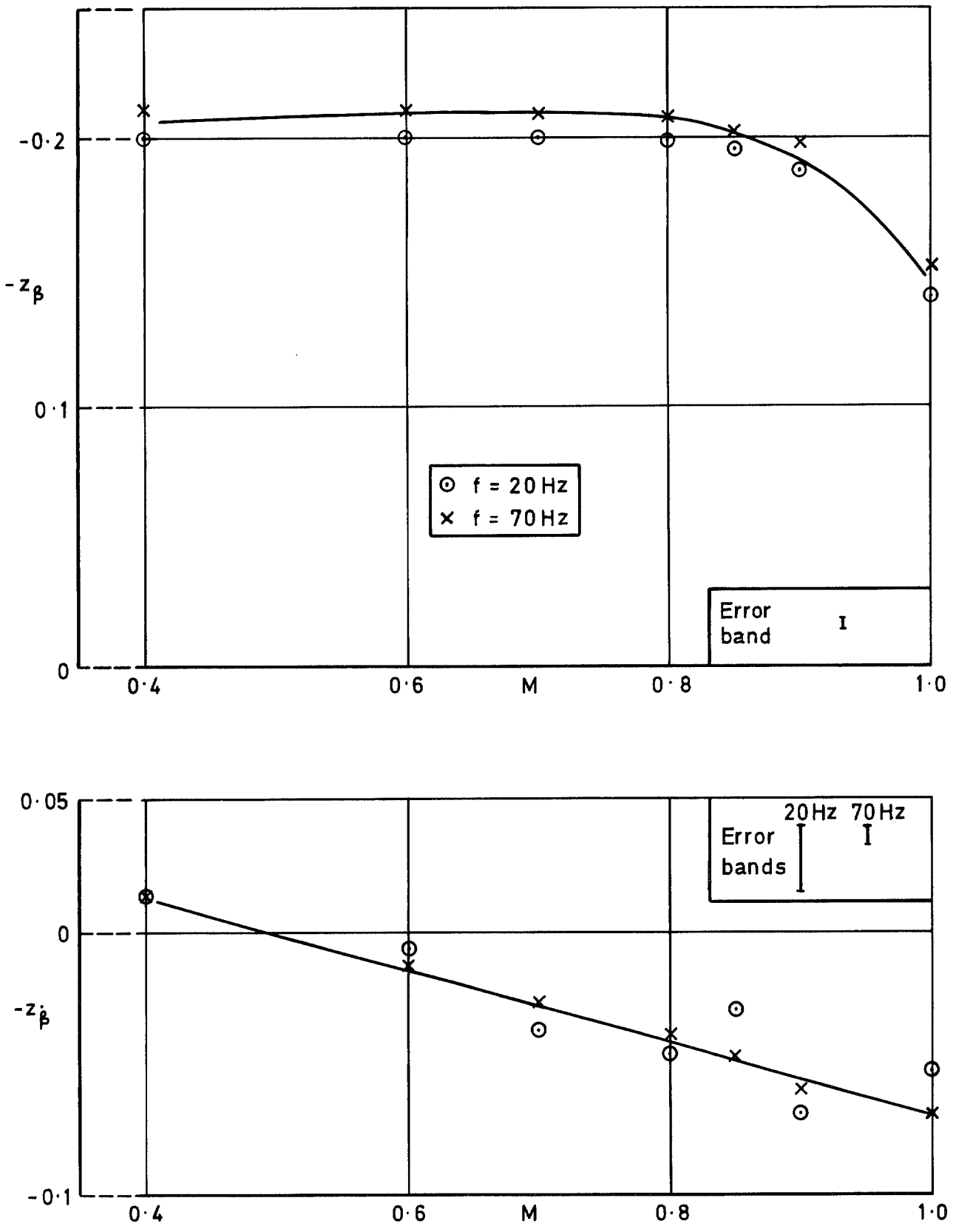

FIG. 4. Variation of normal force derivatives with Mach number. Larger tunnel.

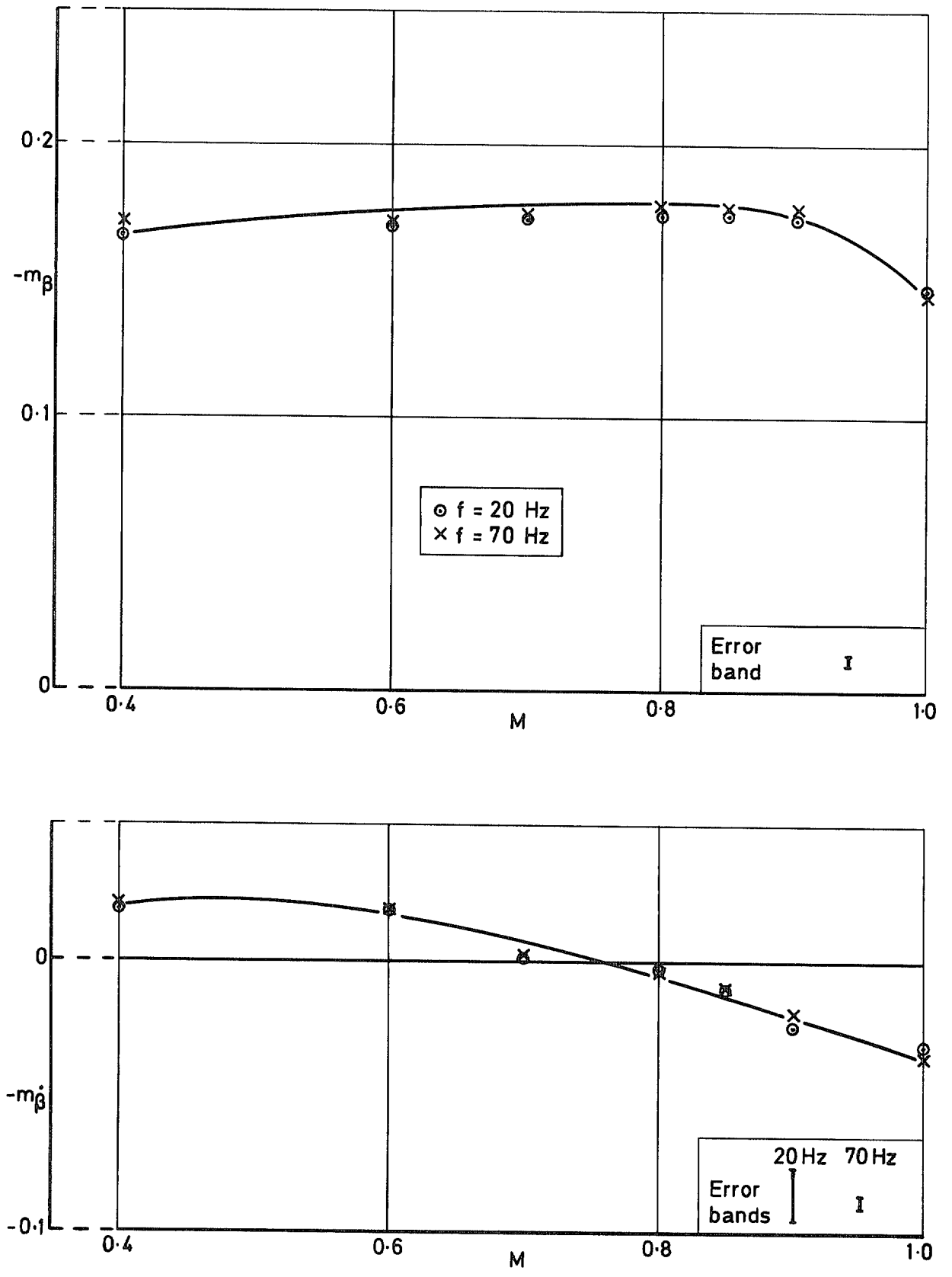

FIG. 5. Variation of pitching moment derivatives with Mach number. Larger tunnel.

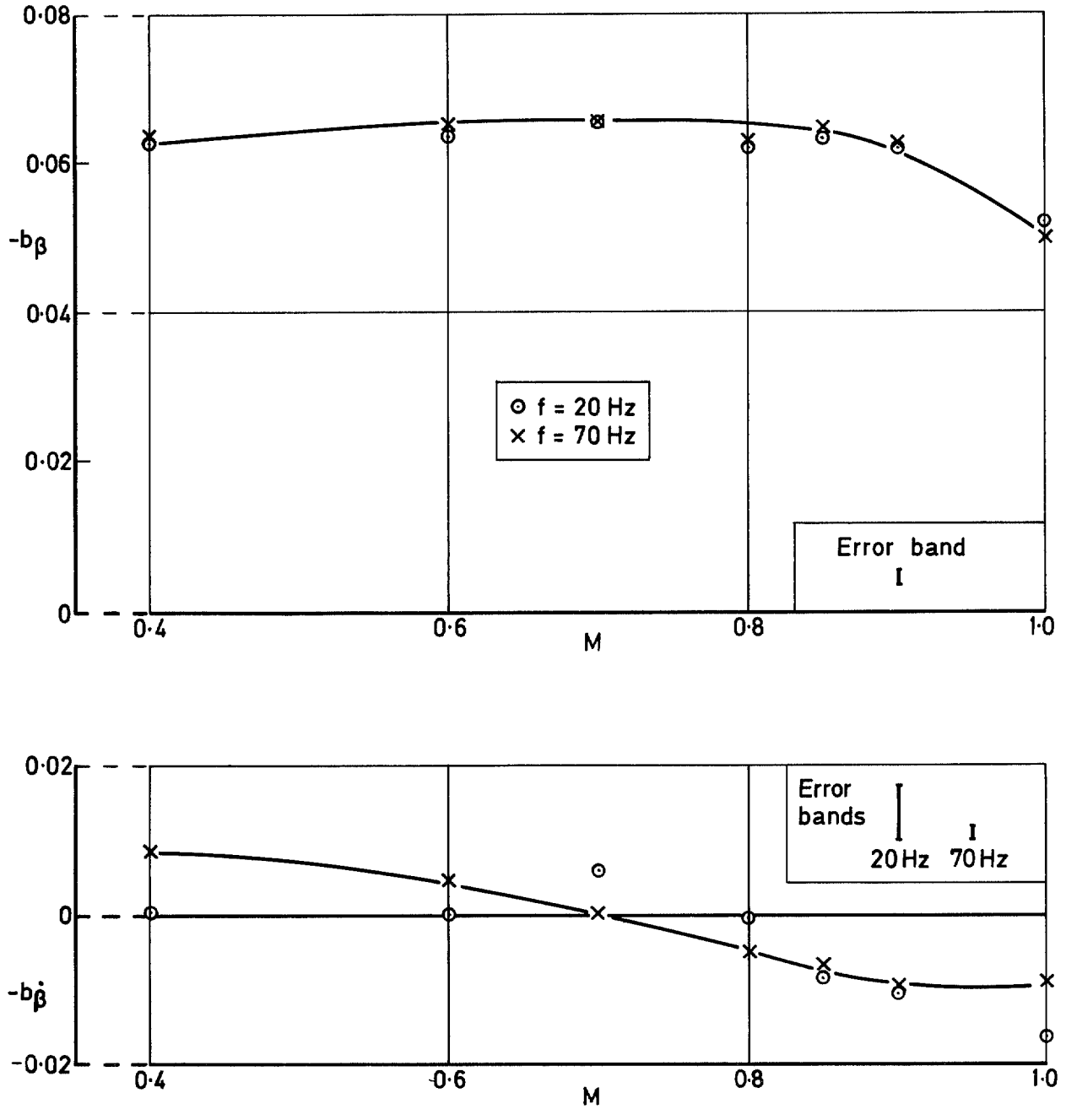

FIG. 6. Variation of bending moment derivatives with Mach number. Larger tunnel.

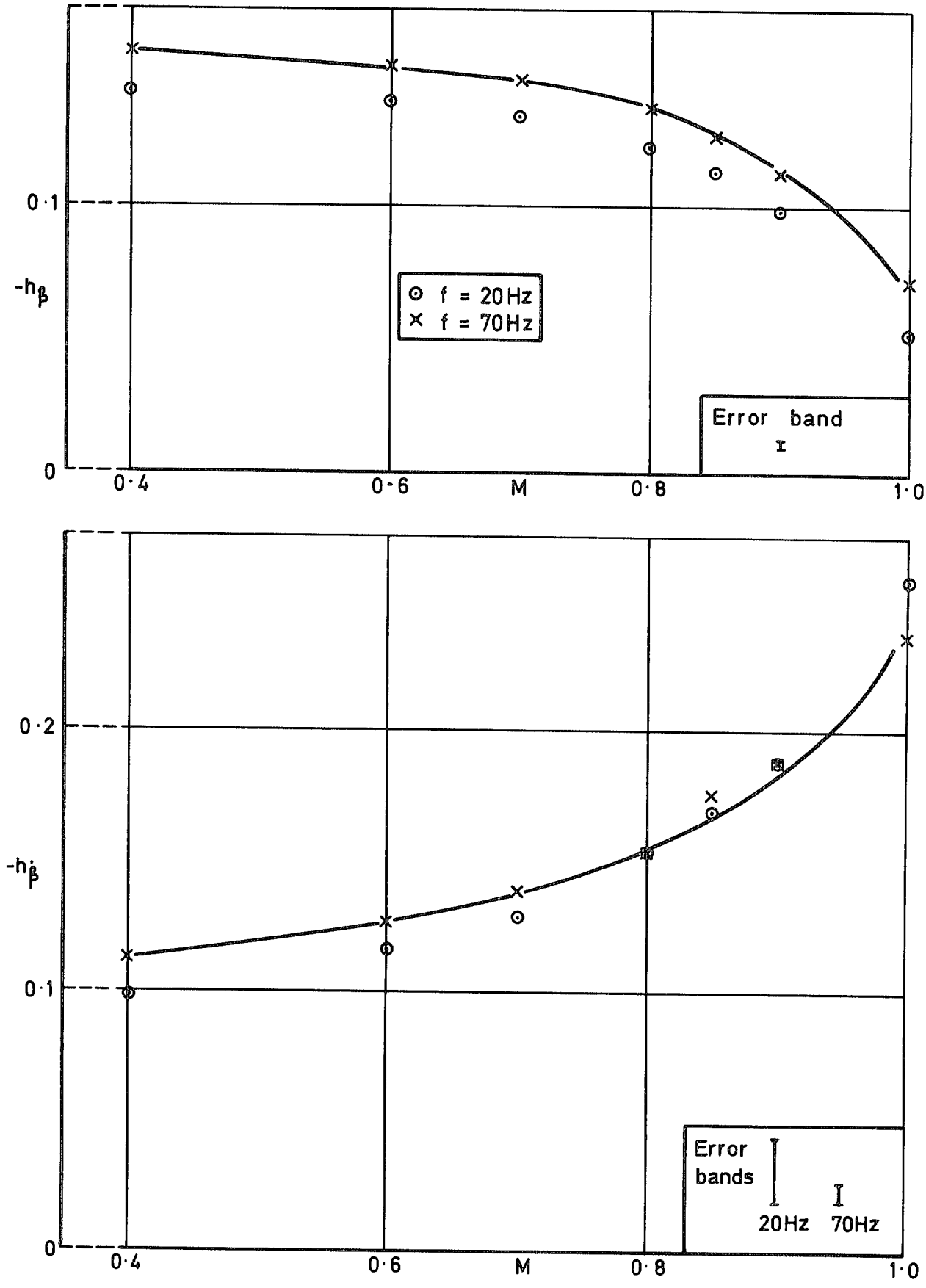

FIG. 7. Variation of hinge moment derivatives with Mach number. Larger tunnel.

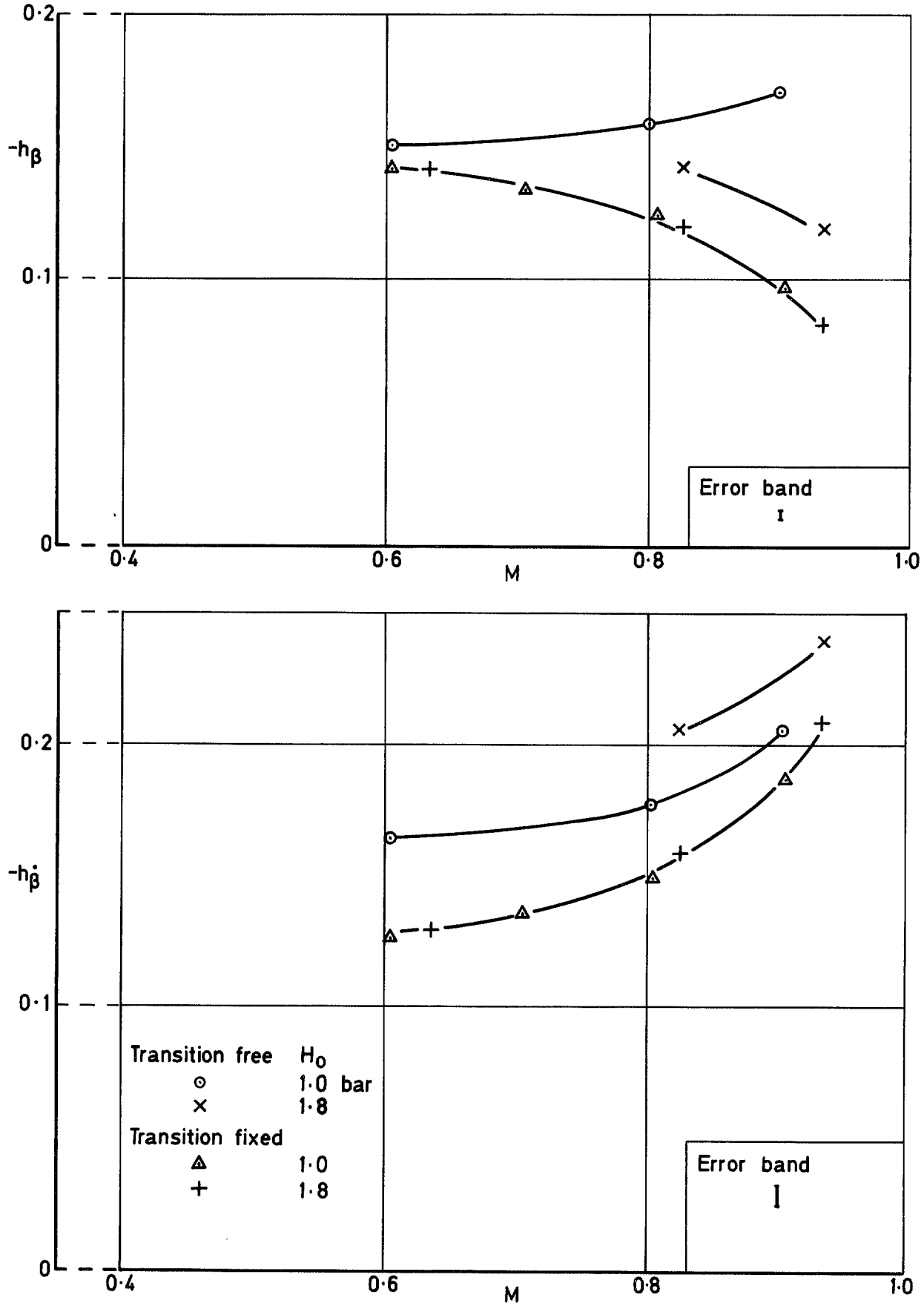

FIG. 8. Effect of transition fixing and tunnel stagnation pressure on hinge moment derivatives. Smaller tunnel.

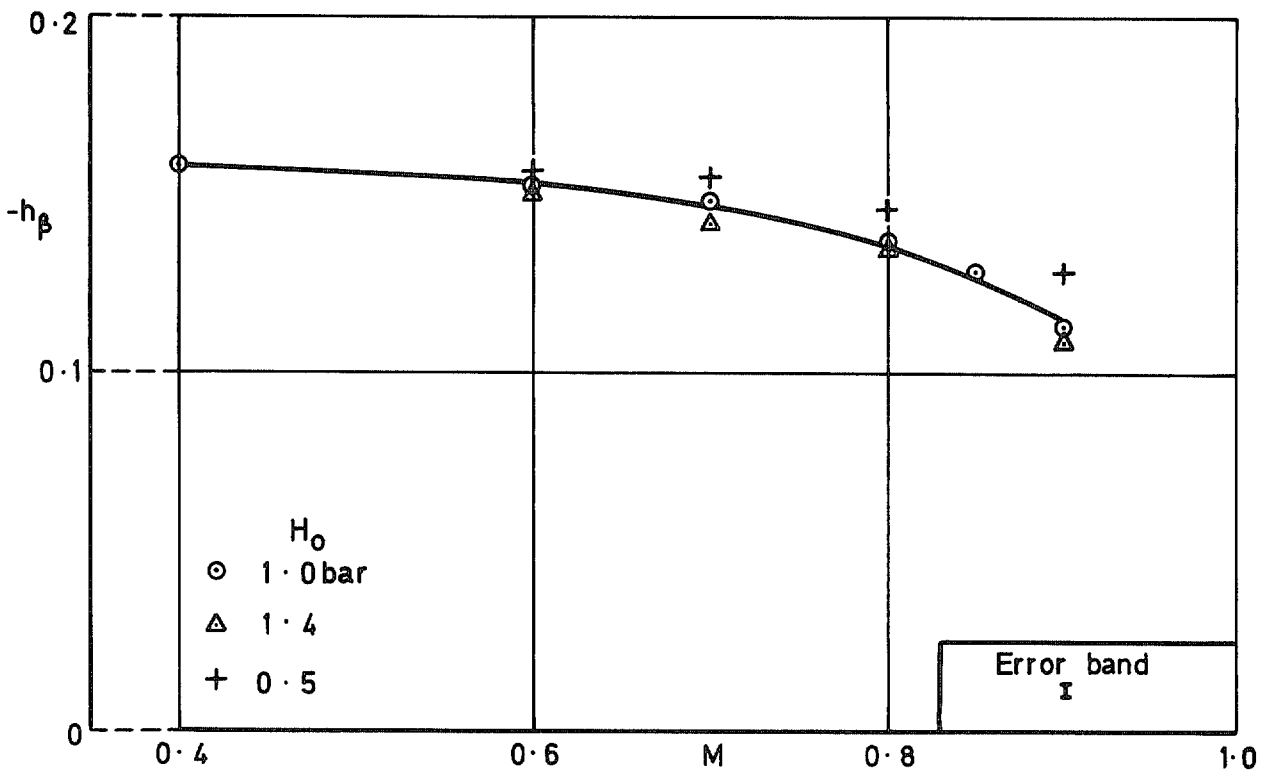

FIG. 9. Effect of tunnel stagnation pressure on hinge moment stiffness. With transition band in larger tunnel.

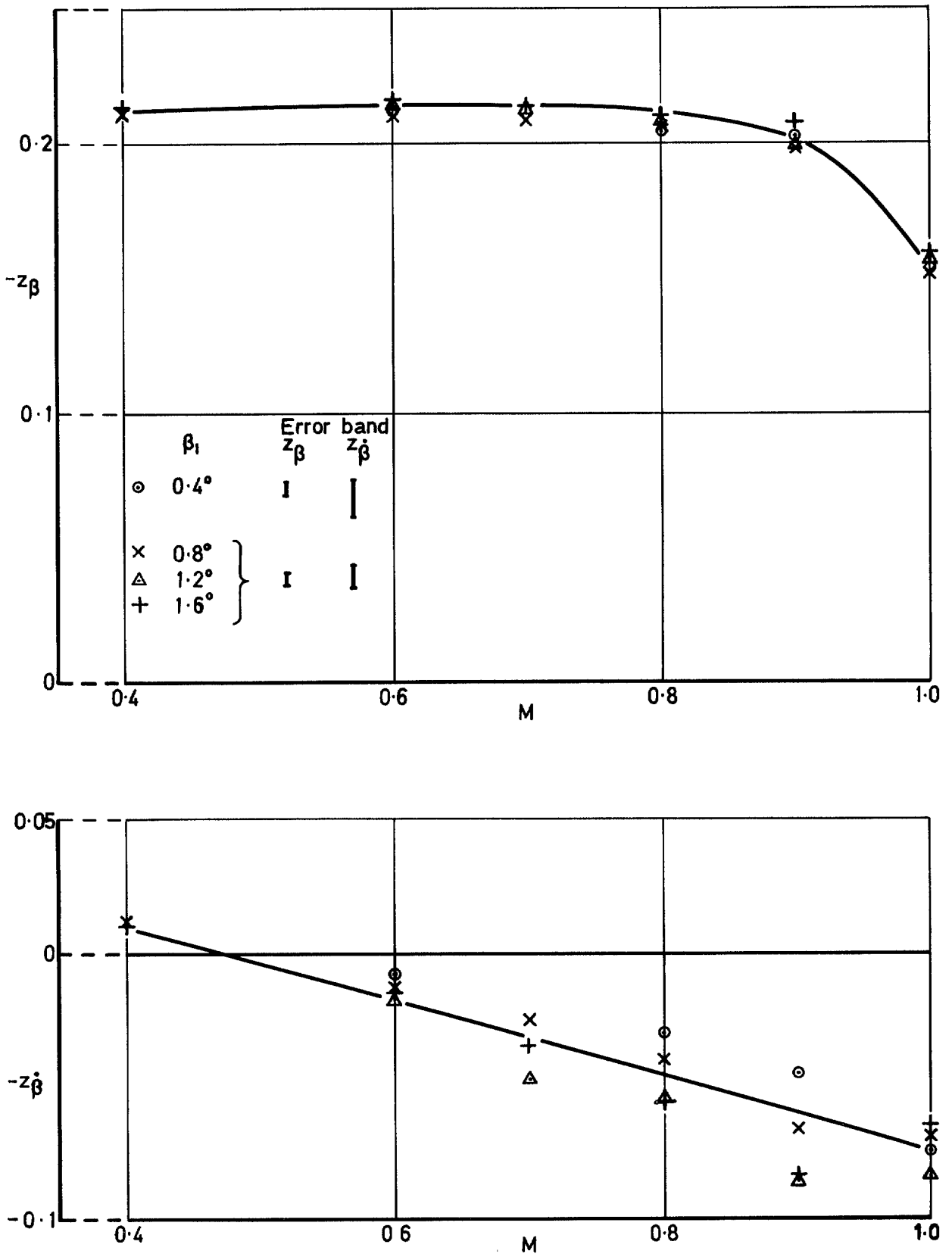

FIG. 10. Effect of control—surface amplitude on normal force derivatives. Larger tunnel.

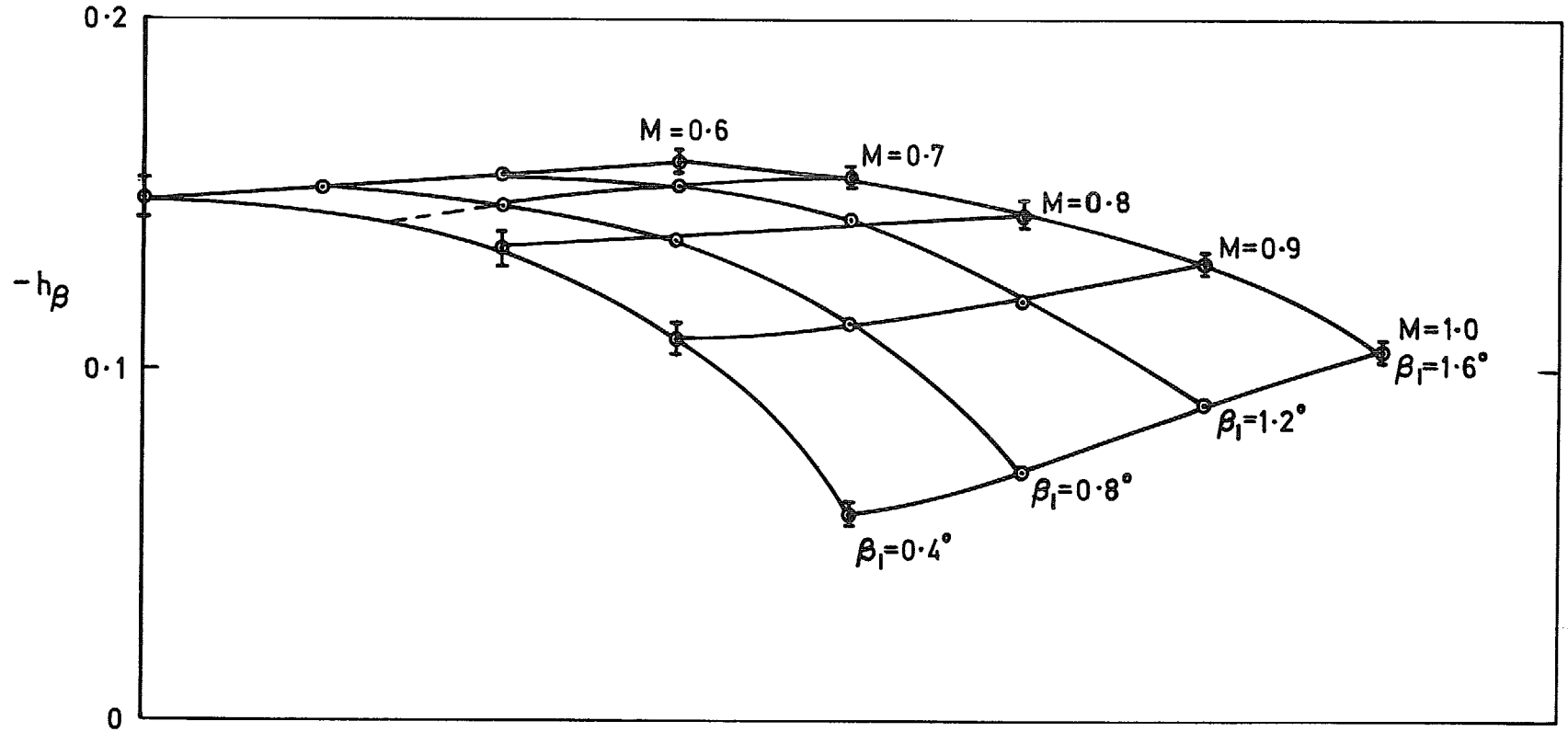

FIG. 11. Effect of control—surface amplitude on hinge moment stiffness. Larger tunnel.

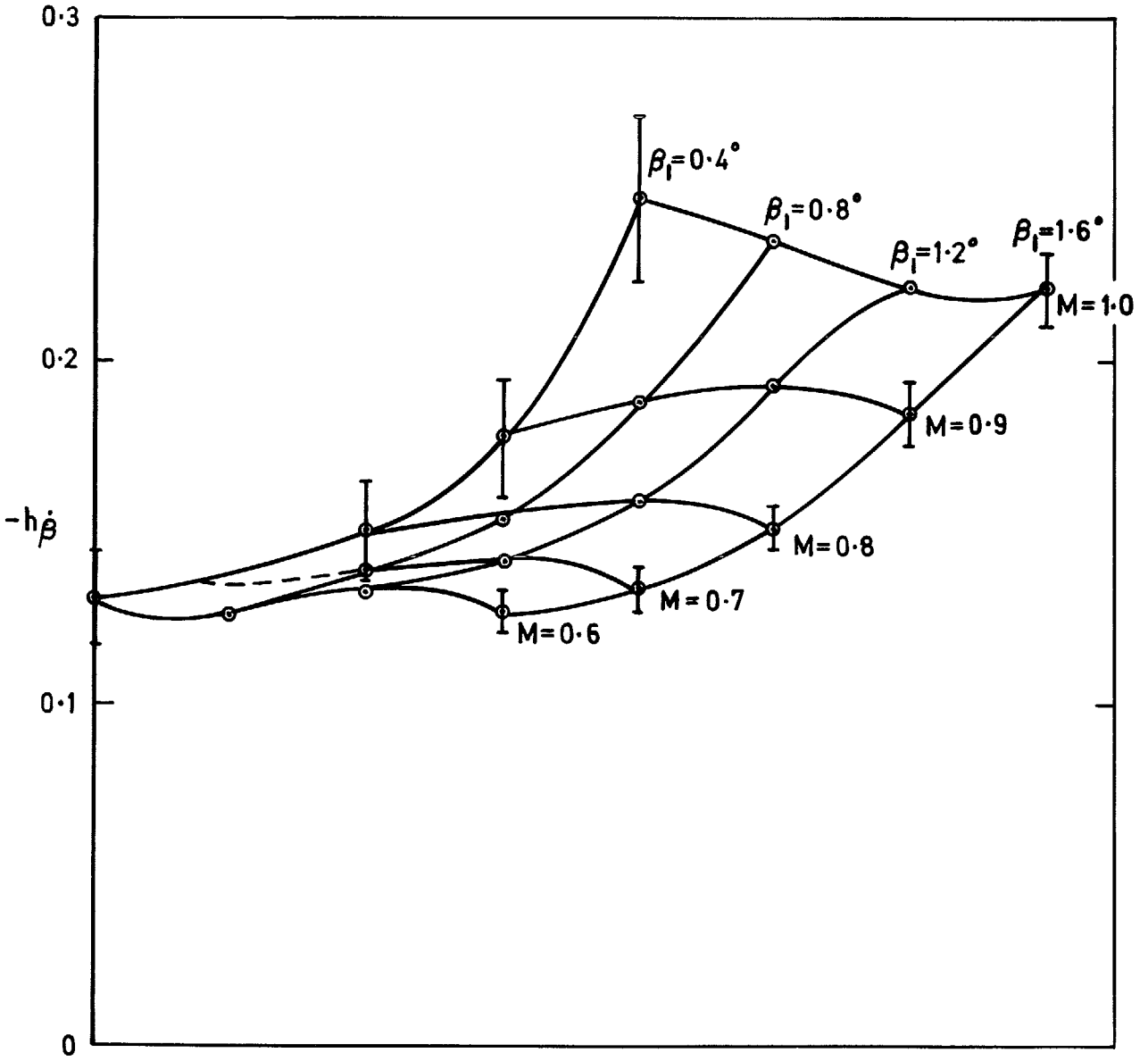

FIG. 12. Effect of control—surface amplitude on hinge moment damping. Larger tunnel.

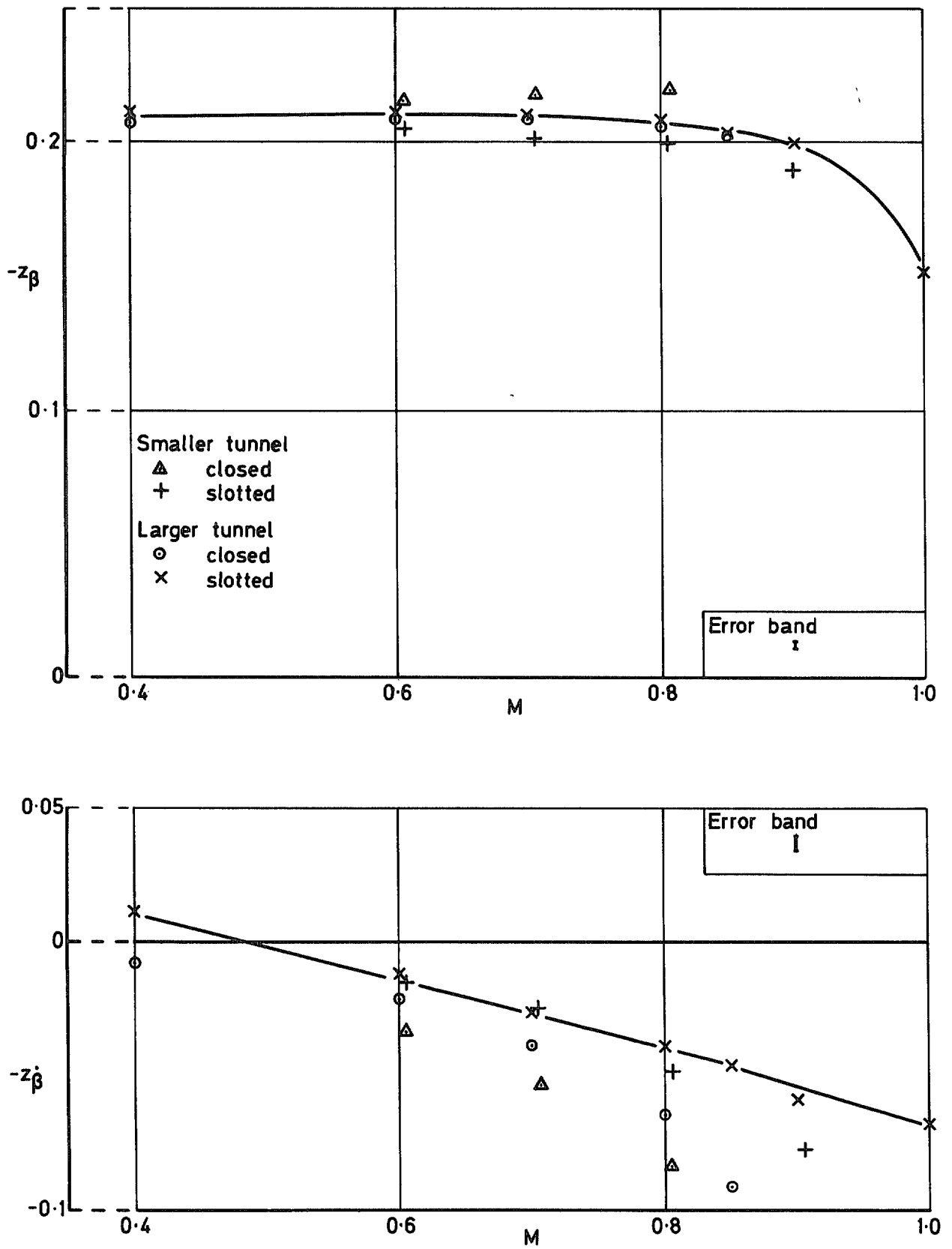

FIG. 13. Effects of different tunnel working sections on normal force derivatives.

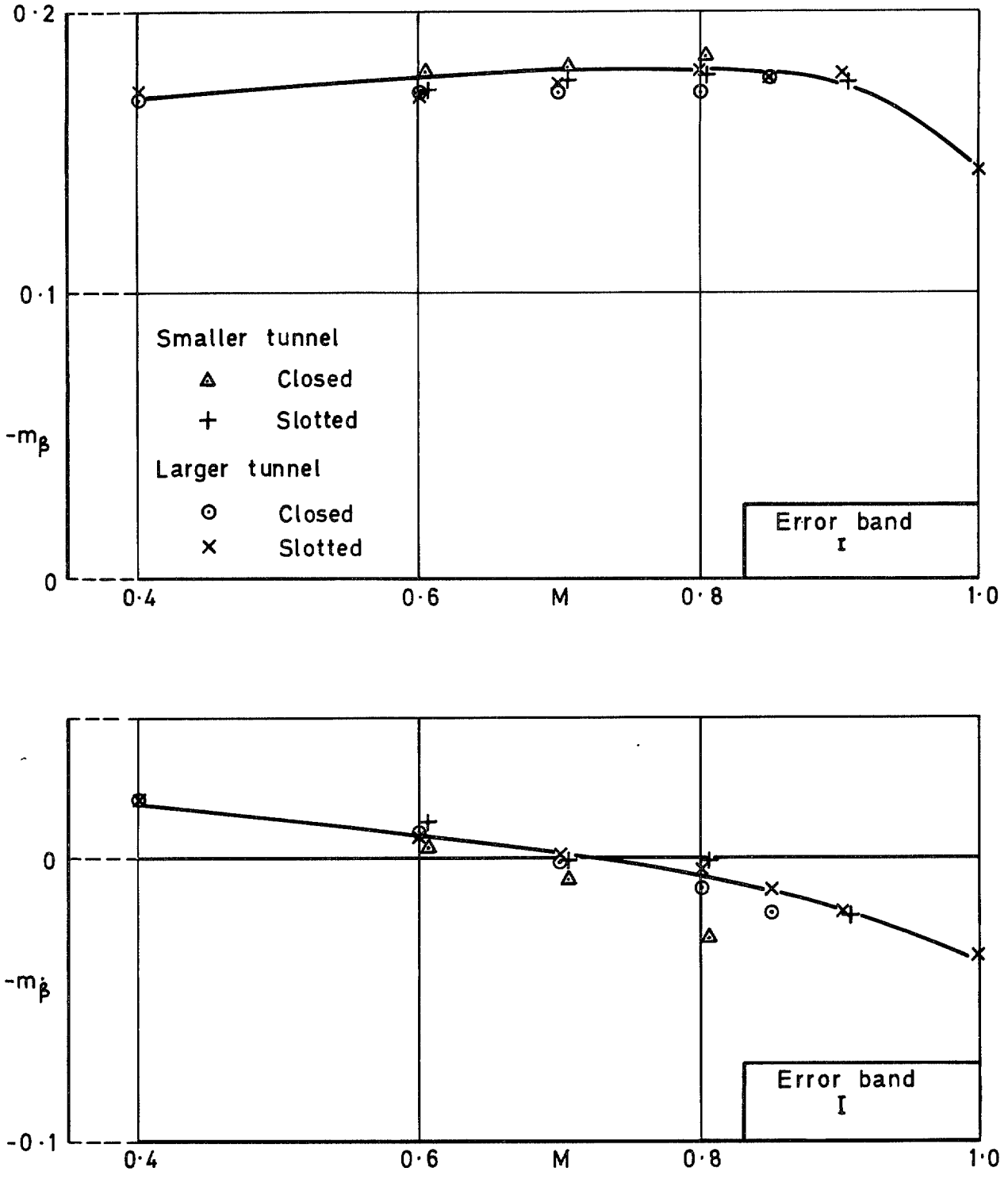

FIG. 14. Effects of different tunnel working sections on pitching moment derivatives.

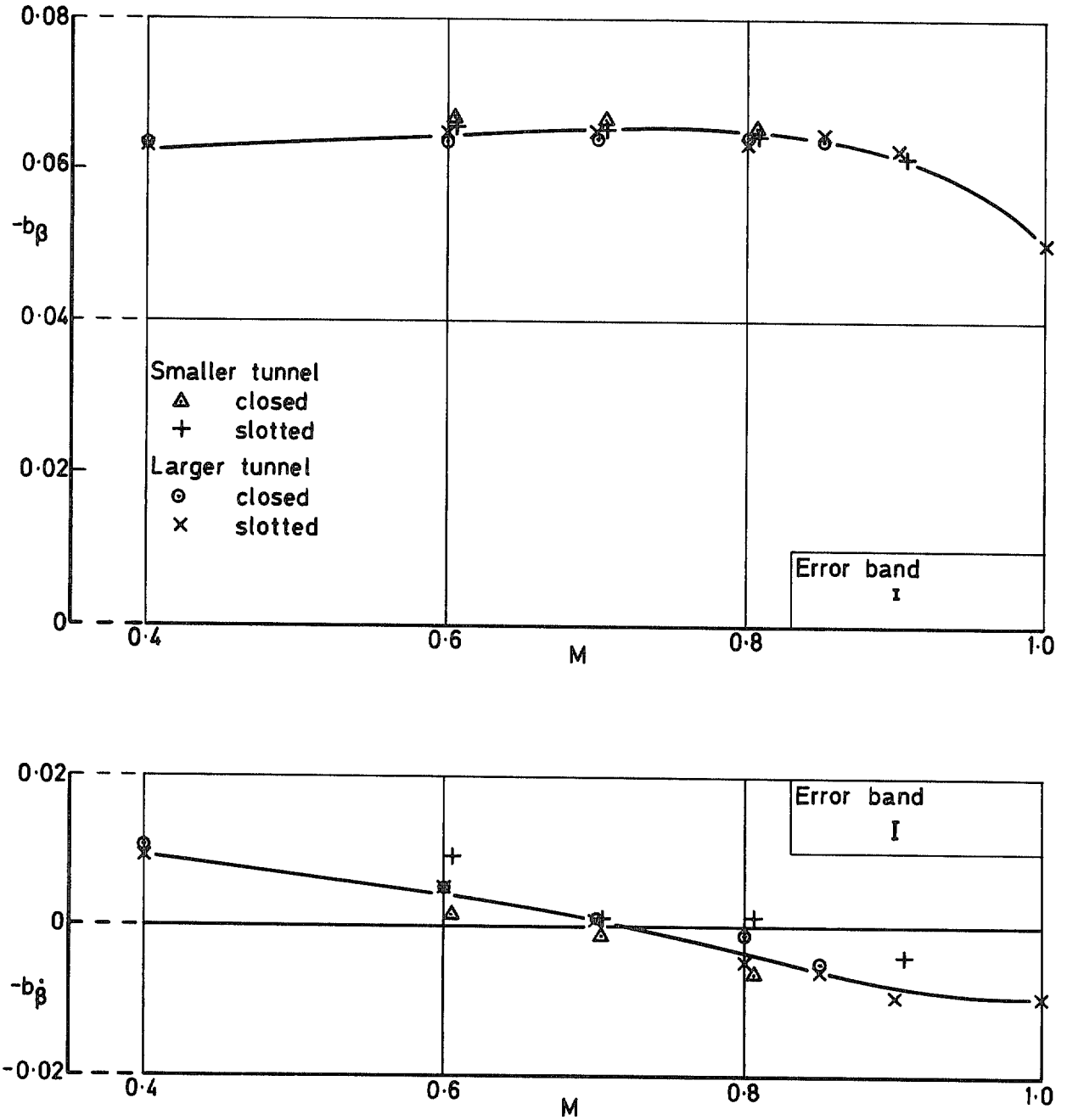

FIG. 15. Effects of different tunnel working sections on bending moment derivatives.

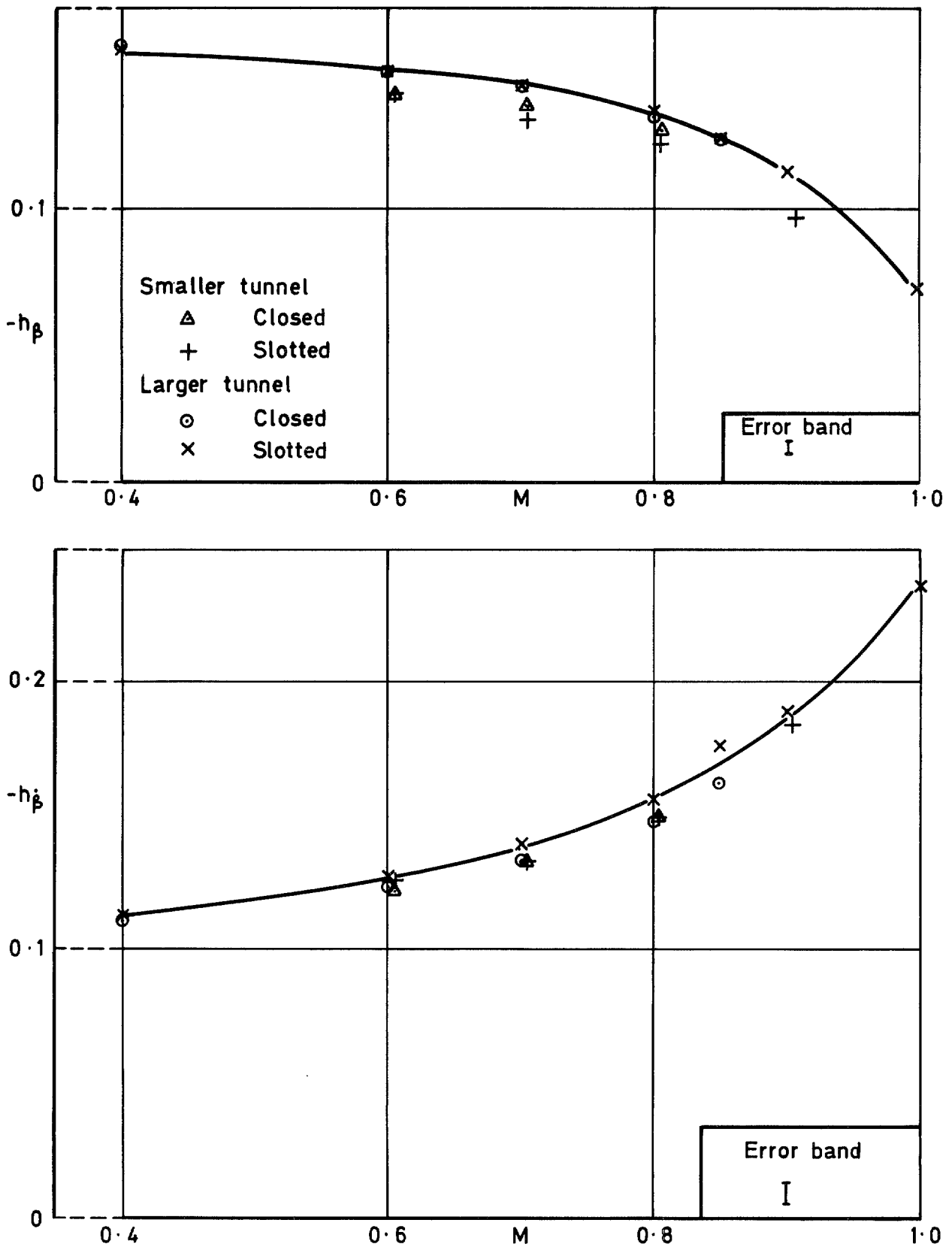

FIG. 16. Effects of different tunnel working sections on hinge moment derivatives

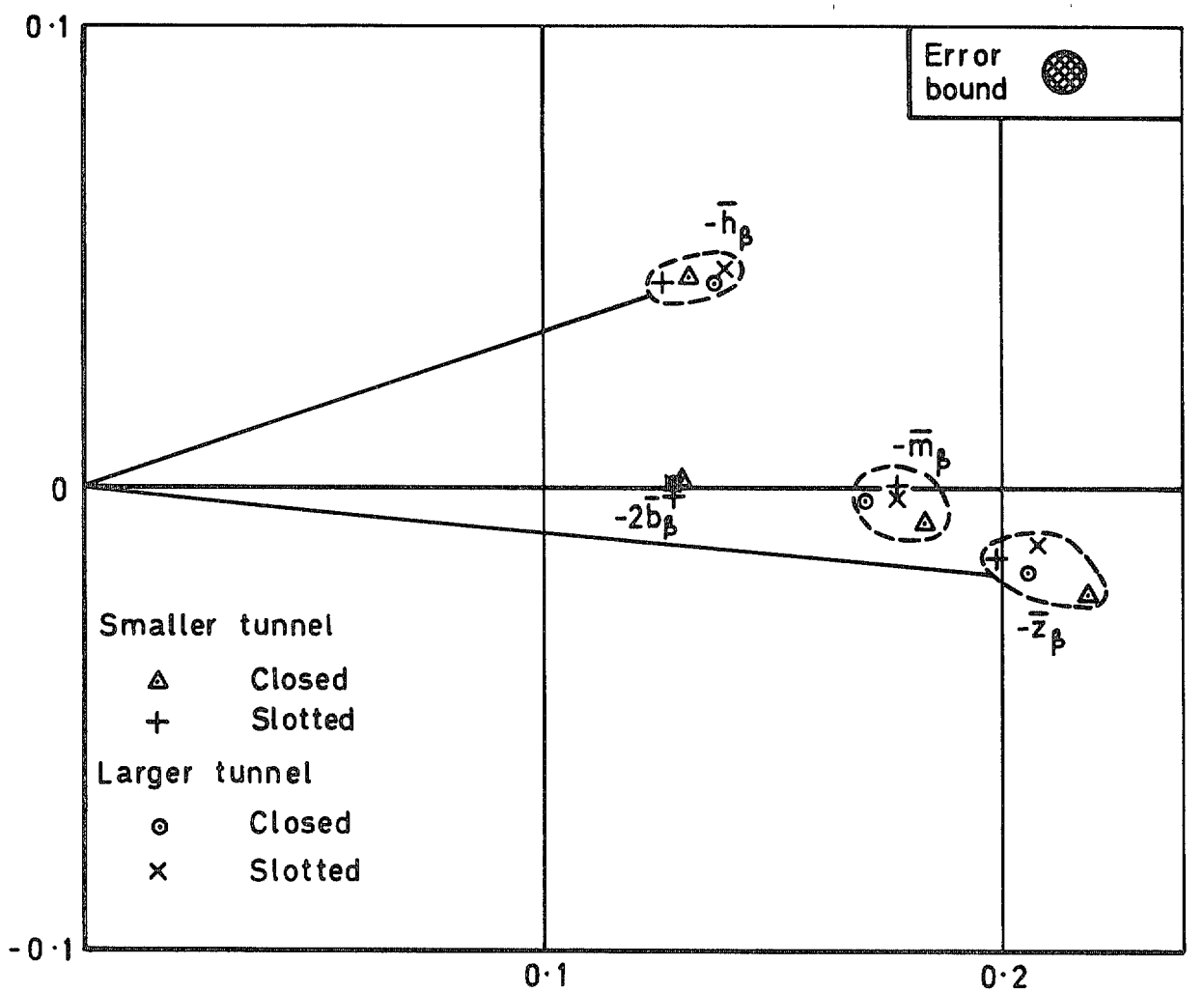

FIG. 17. Complex derivatives for $M = 0{\cdot}781$, $\bar{\nu} = 0{\cdot}32$, interpolated from measurements. Before correction for tunnel interference.

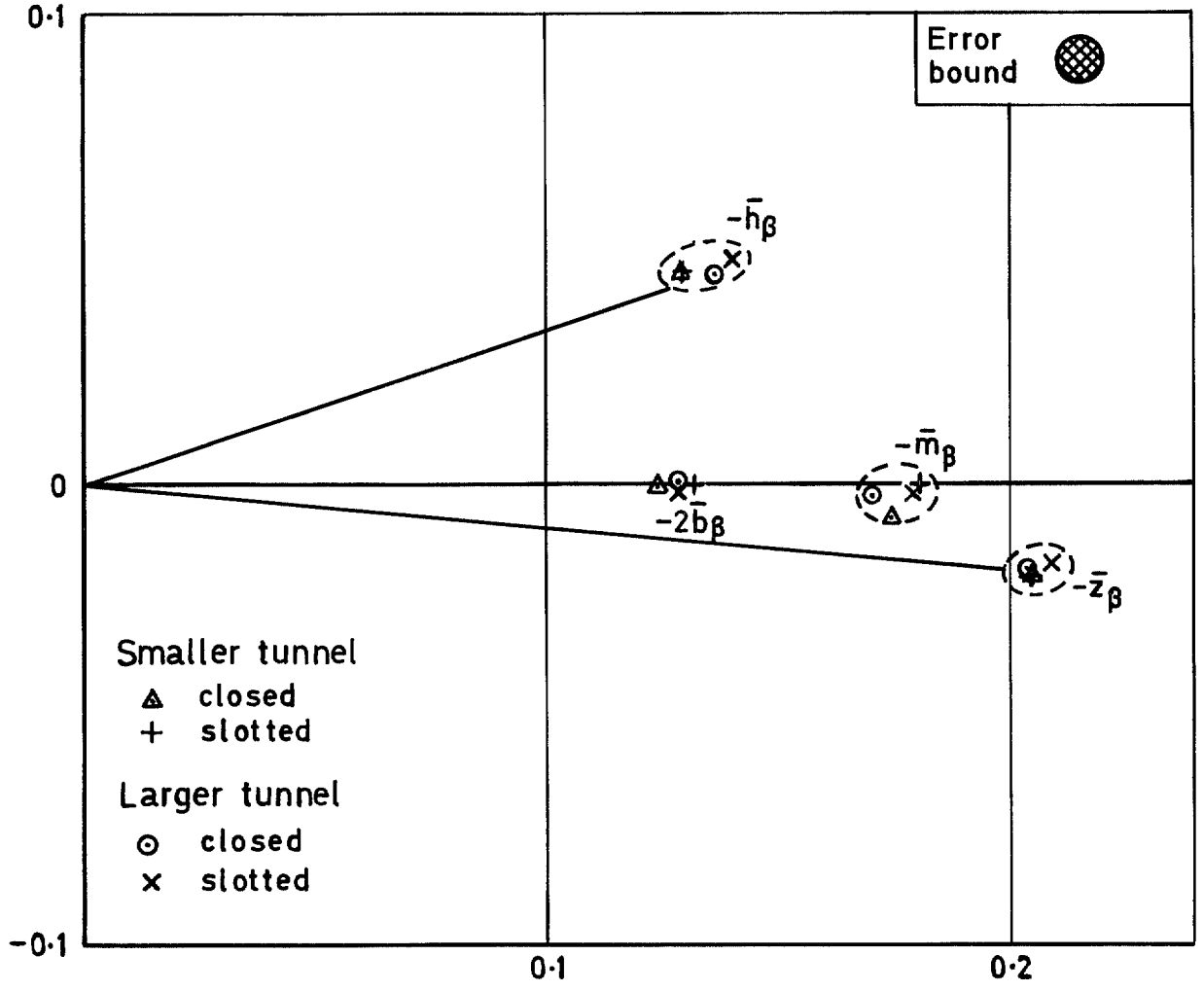

FIG. 18. Complex derivatives for $M = 0{\cdot}781$, $\bar{\nu} = 0{\cdot}32$, interpolated from measurements. After correction for tunnel interference.

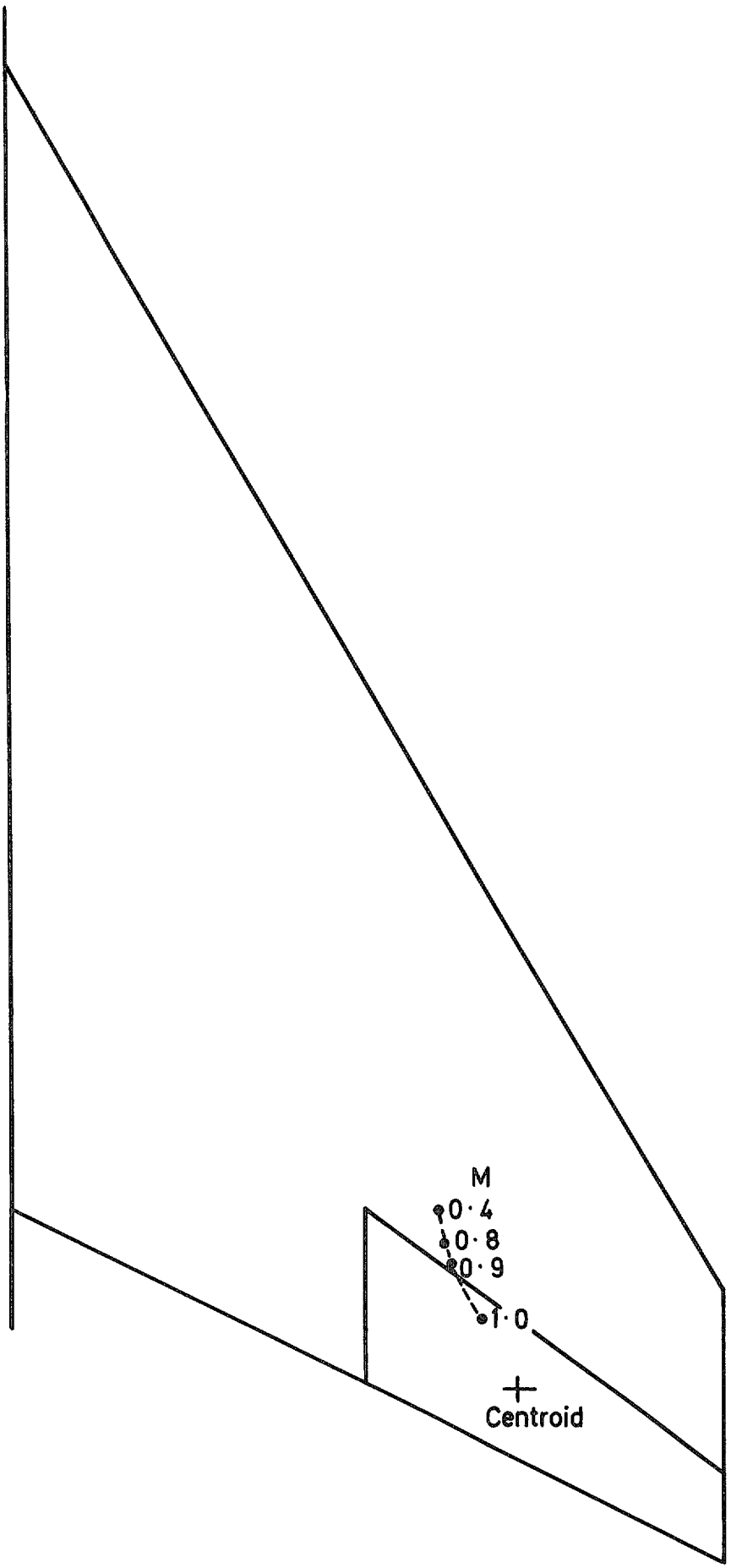

FIG. 19. Centre of action of inphase normal force. Variation with Mach number.

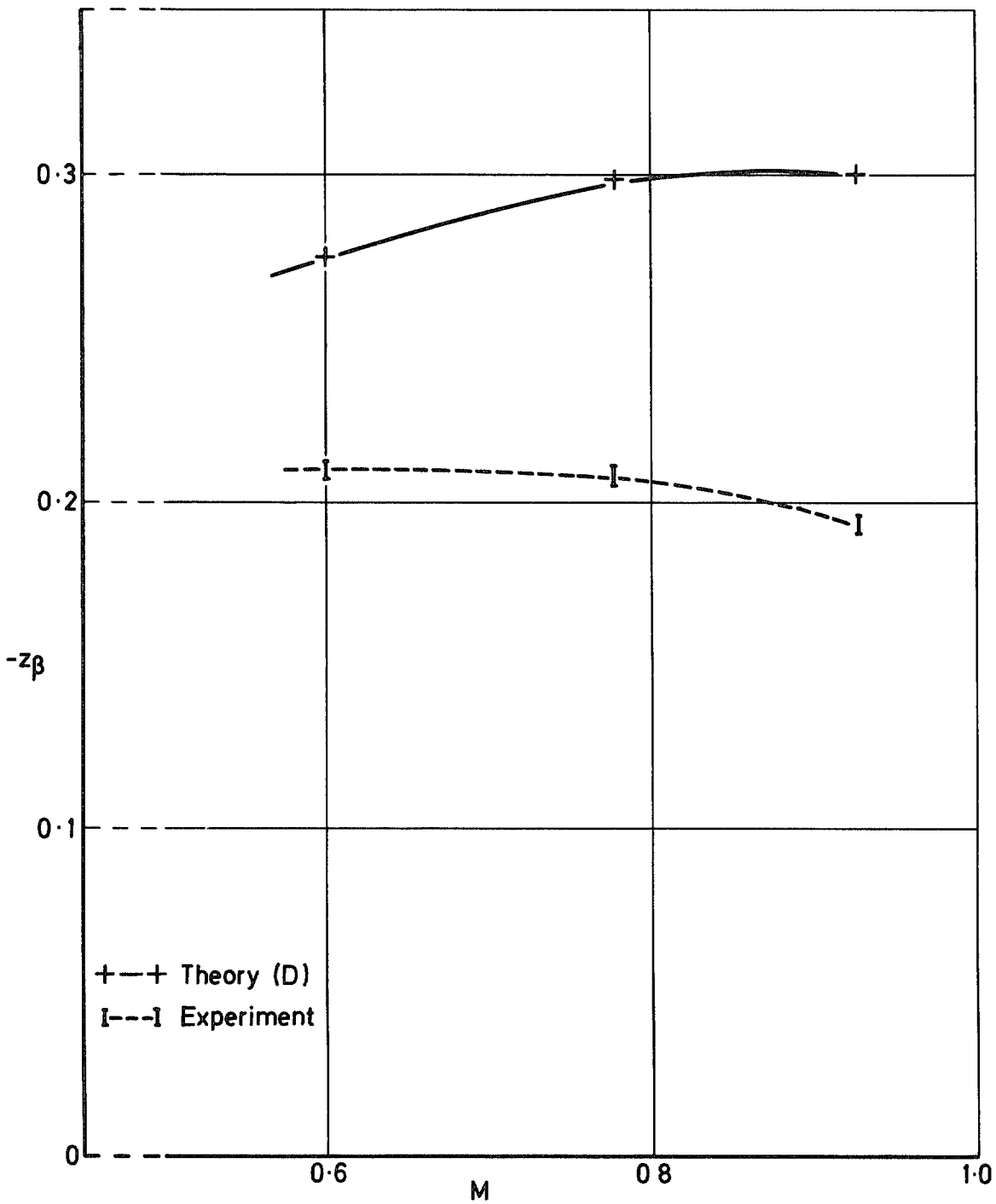

FIG. 20. Comparison of theory and experiment. Normal force stiffness derivative.

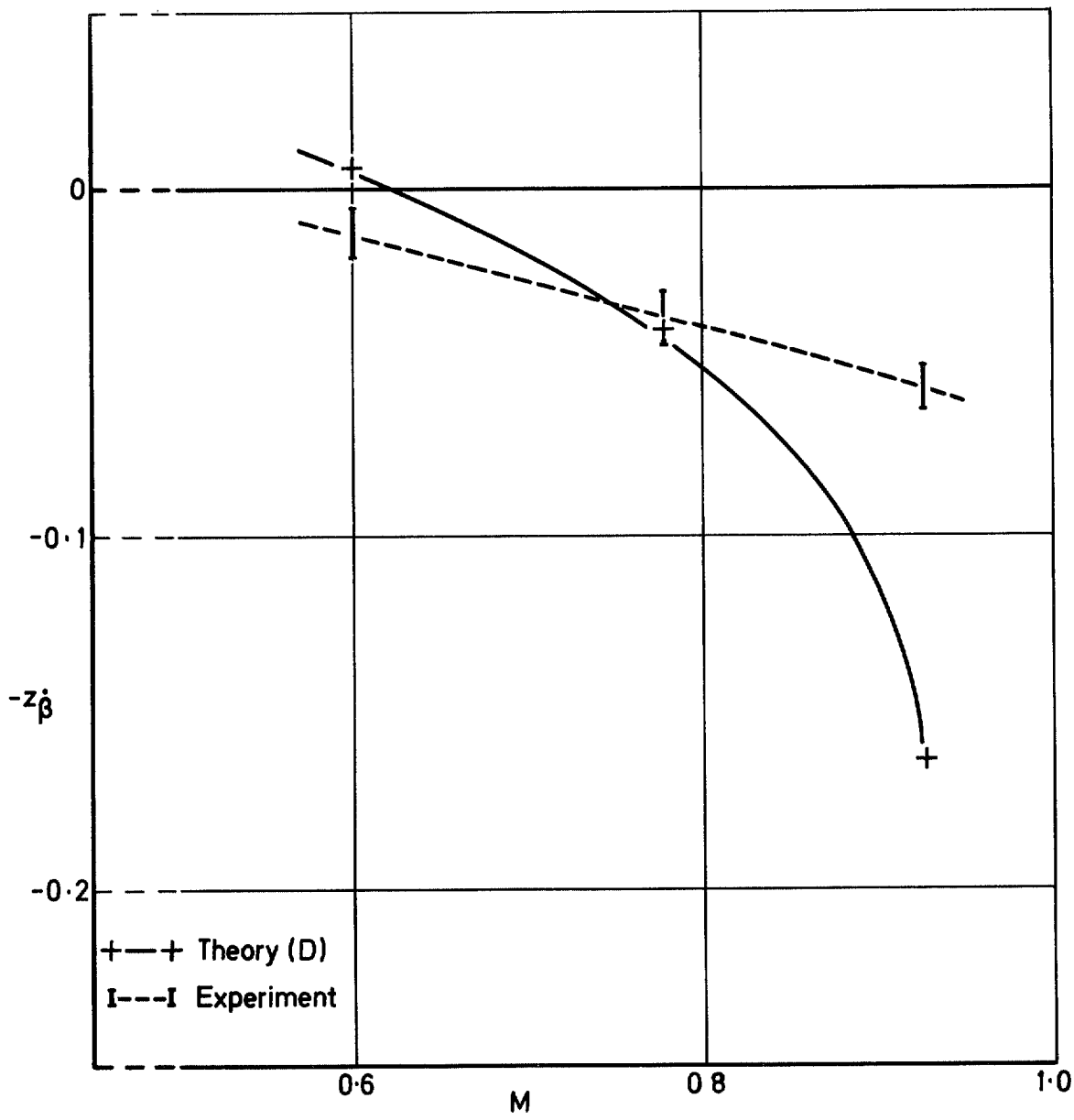

FIG. 21. Comparison of theory and experiment. Normal force damping derivative.

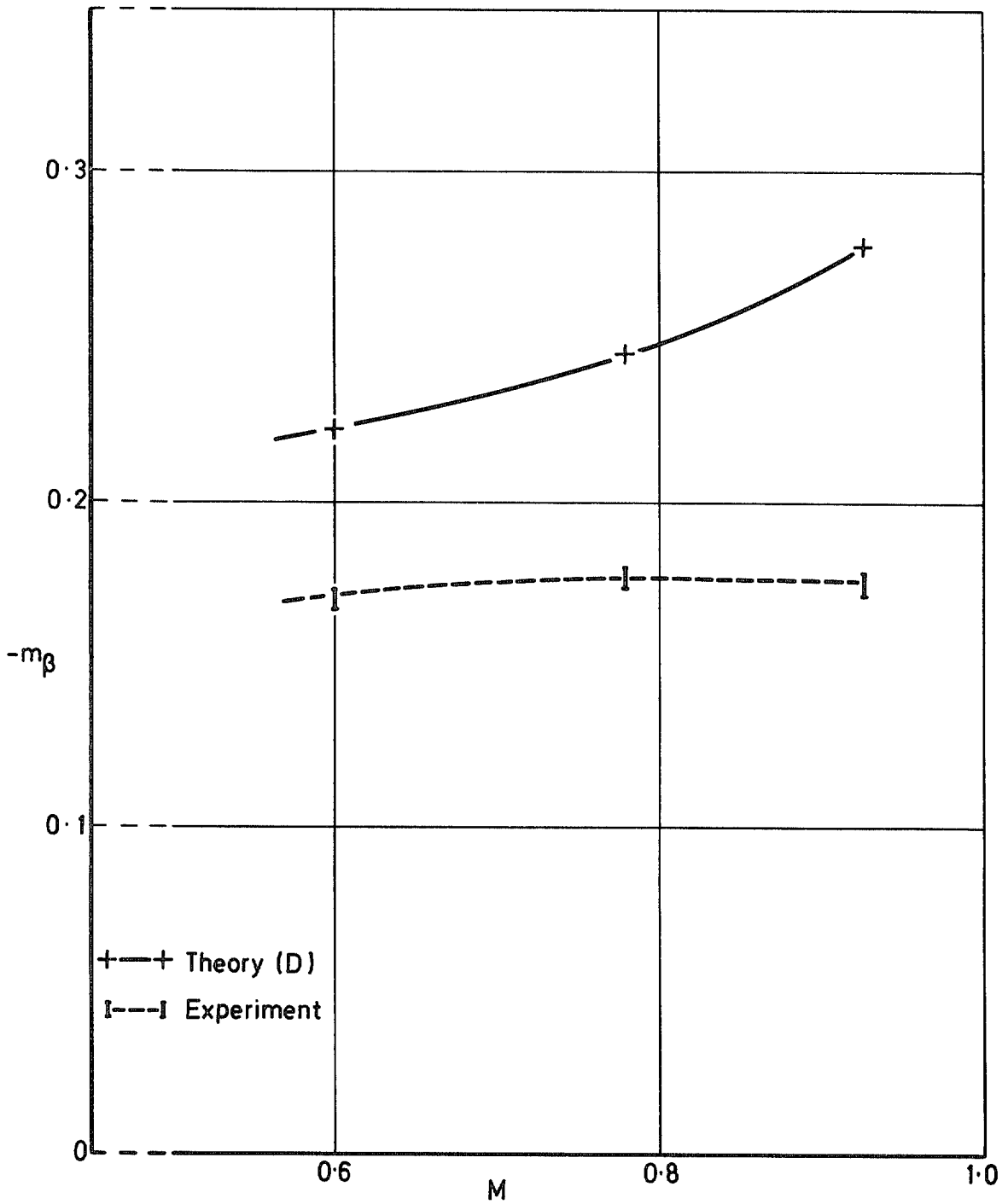

FIG. 22. Comparison of theory and experiment. Pitching moment stiffness derivative.

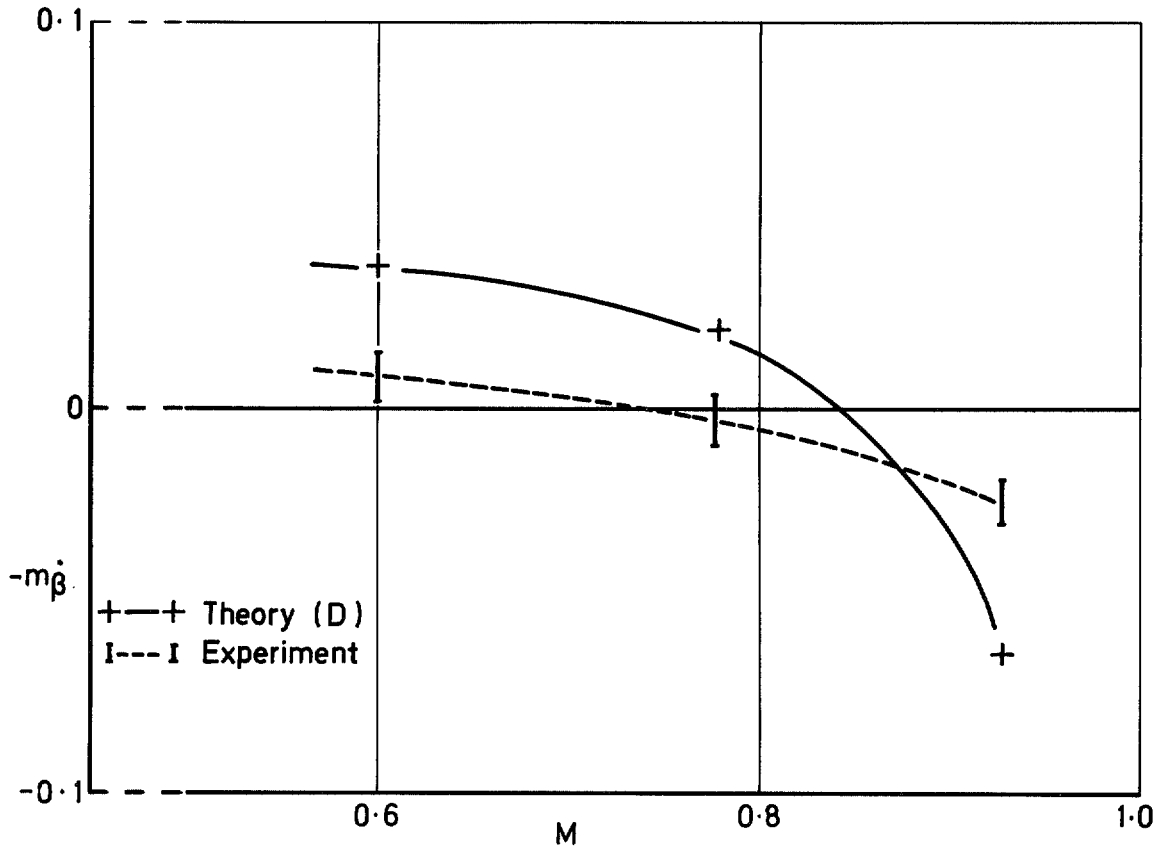

FIG. 23. Comparison of theory and experiment. Pitching moment damping derivative.

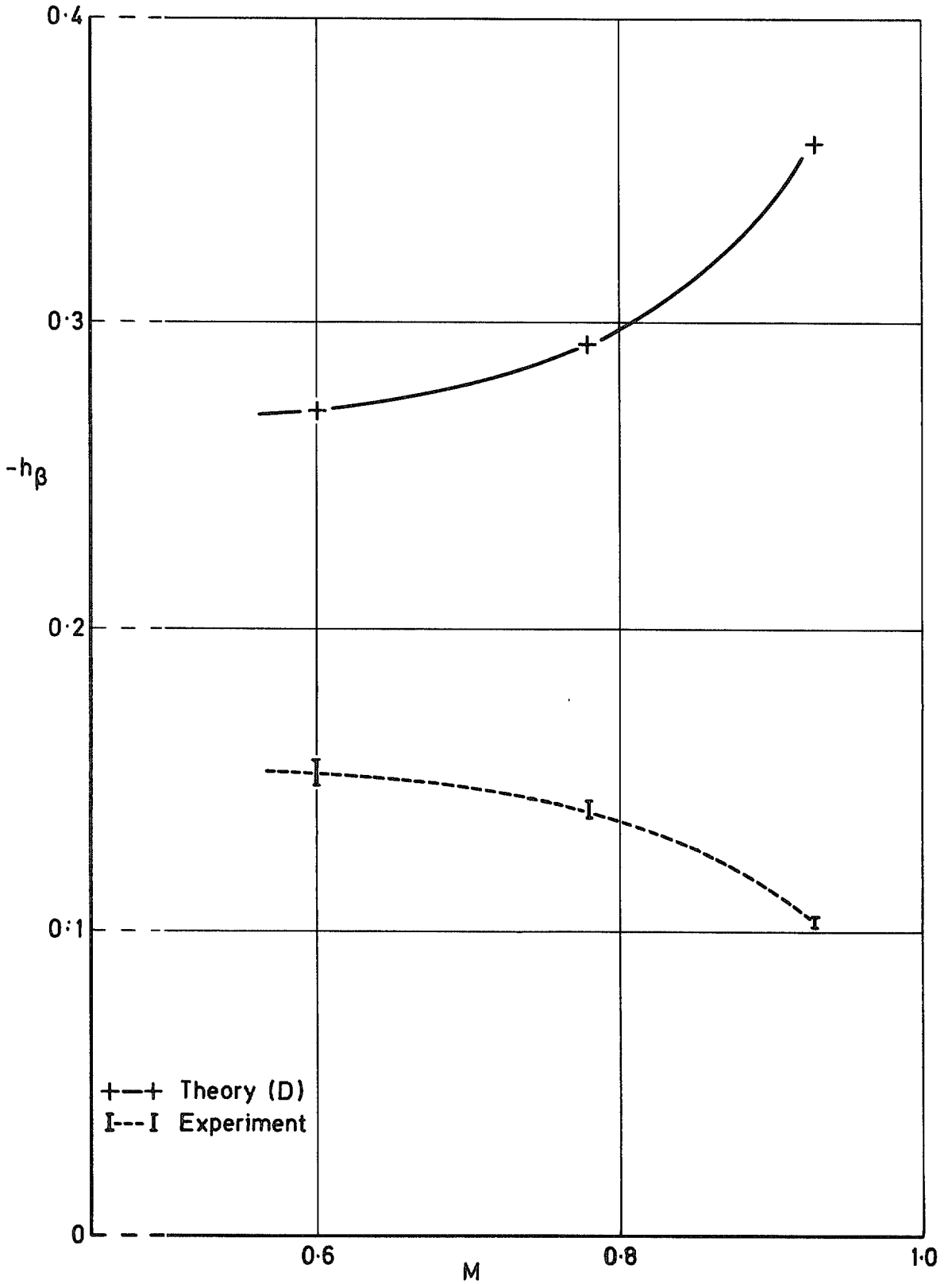

FIG. 24. Comparison of theory and experiment. Hinge moment stiffness derivative.

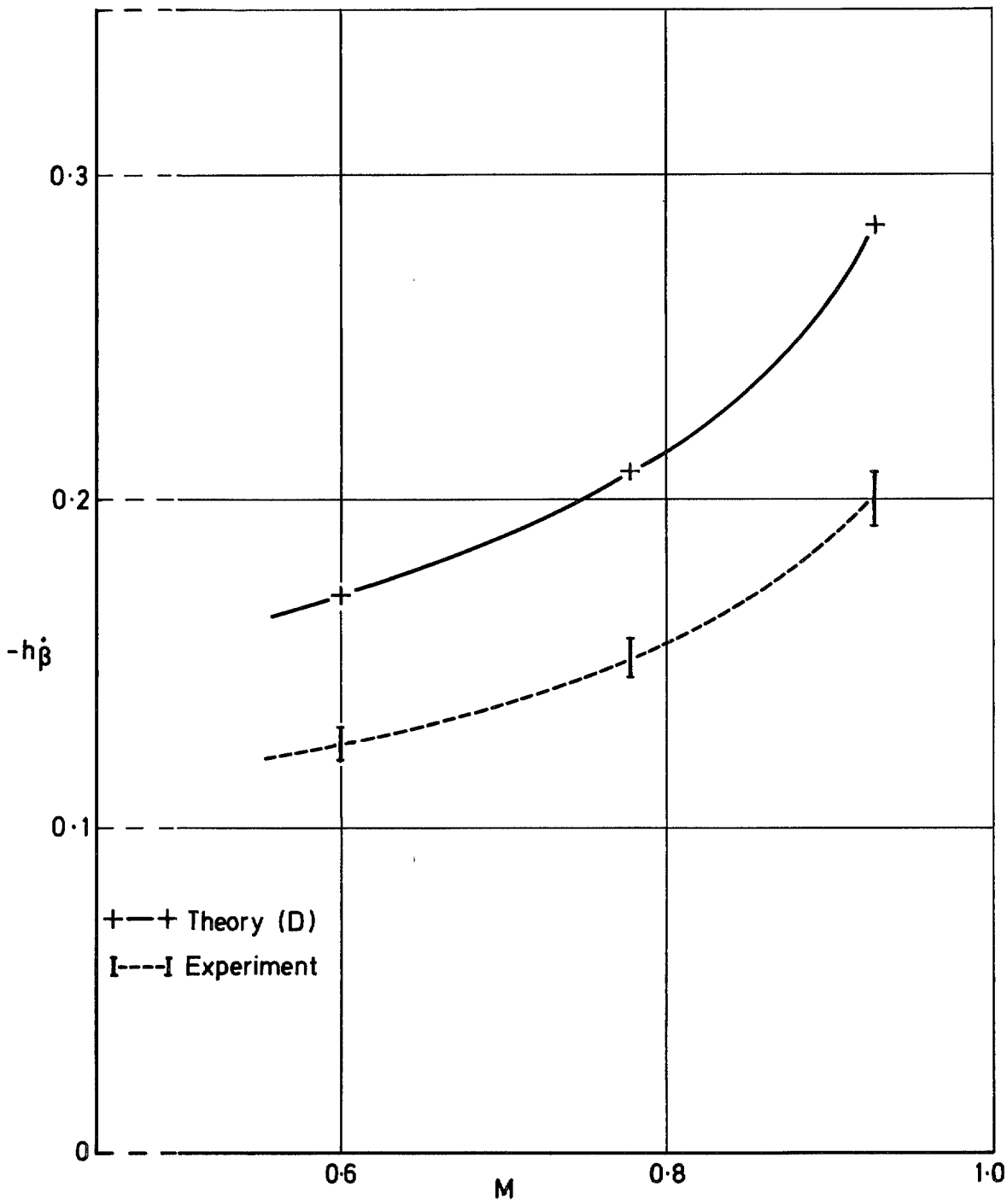

FIG. 25. Comparison of theory and experiment. Hinge moment damping derivative.

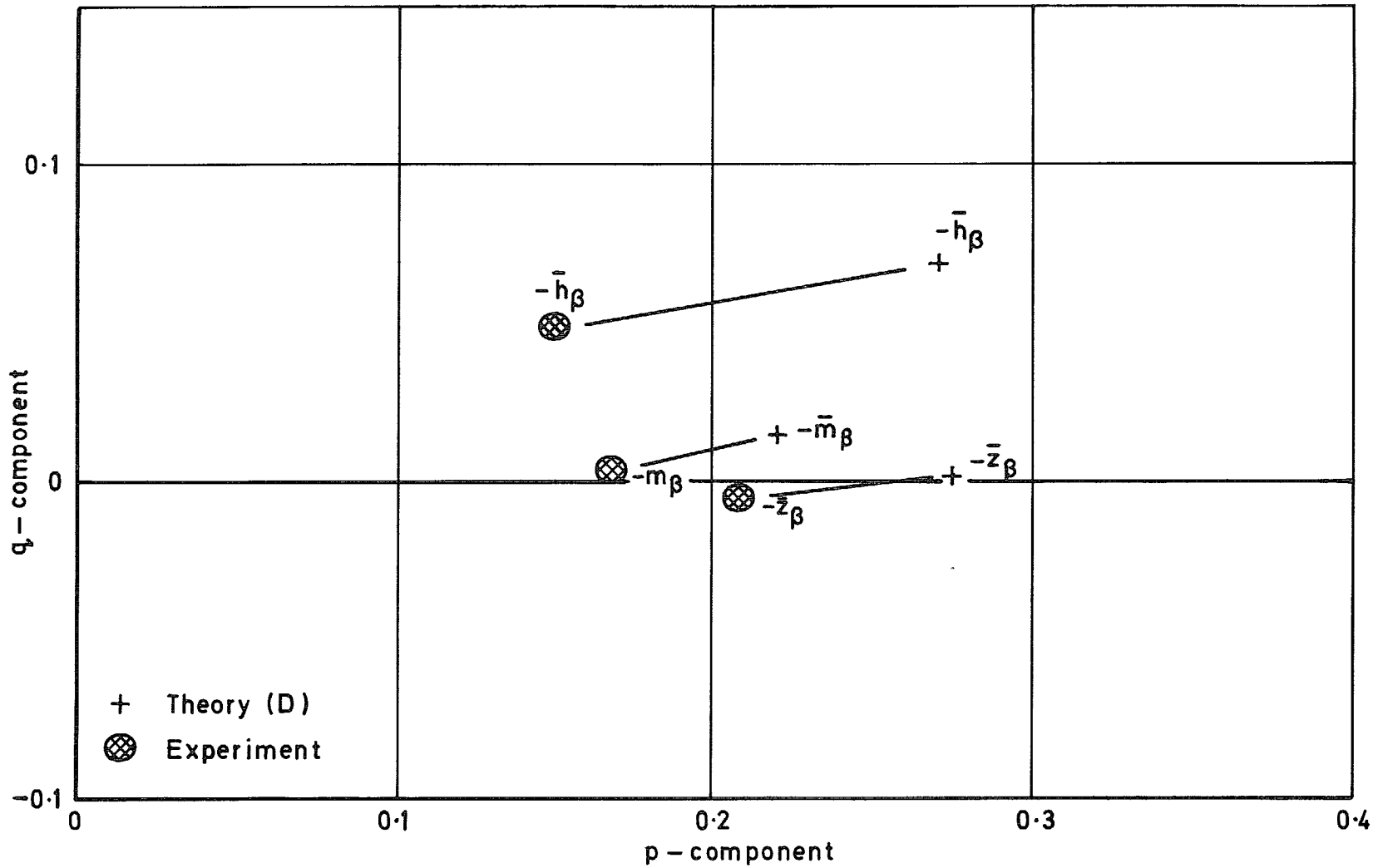

FIG. 26. Comparison of theory and experiment. Complex derivatives for $M = 0.6$, $\bar{\nu} = 0{\cdot}41$.

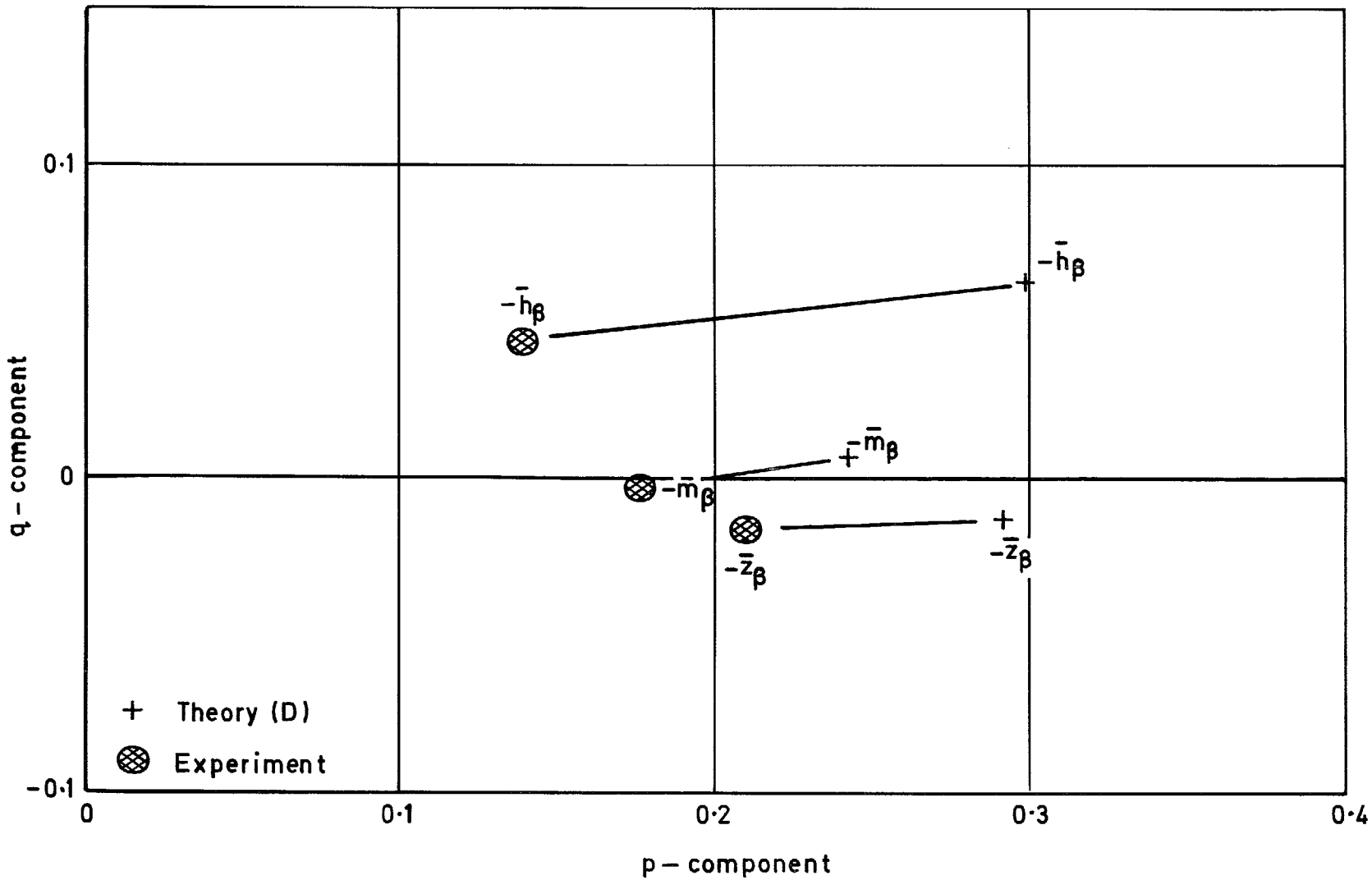

FIG. 27. Comparison of theory and experiment. Complex derivatives for $M = 0{\cdot}781$, $\bar{\nu} = 0{\cdot}32$.

Printed in England for Her Majesty's Stationery Office by J. W. Arrowsmith Ltd., Bristol BS3 2NT
Dd. 587484 K.5. 11/77

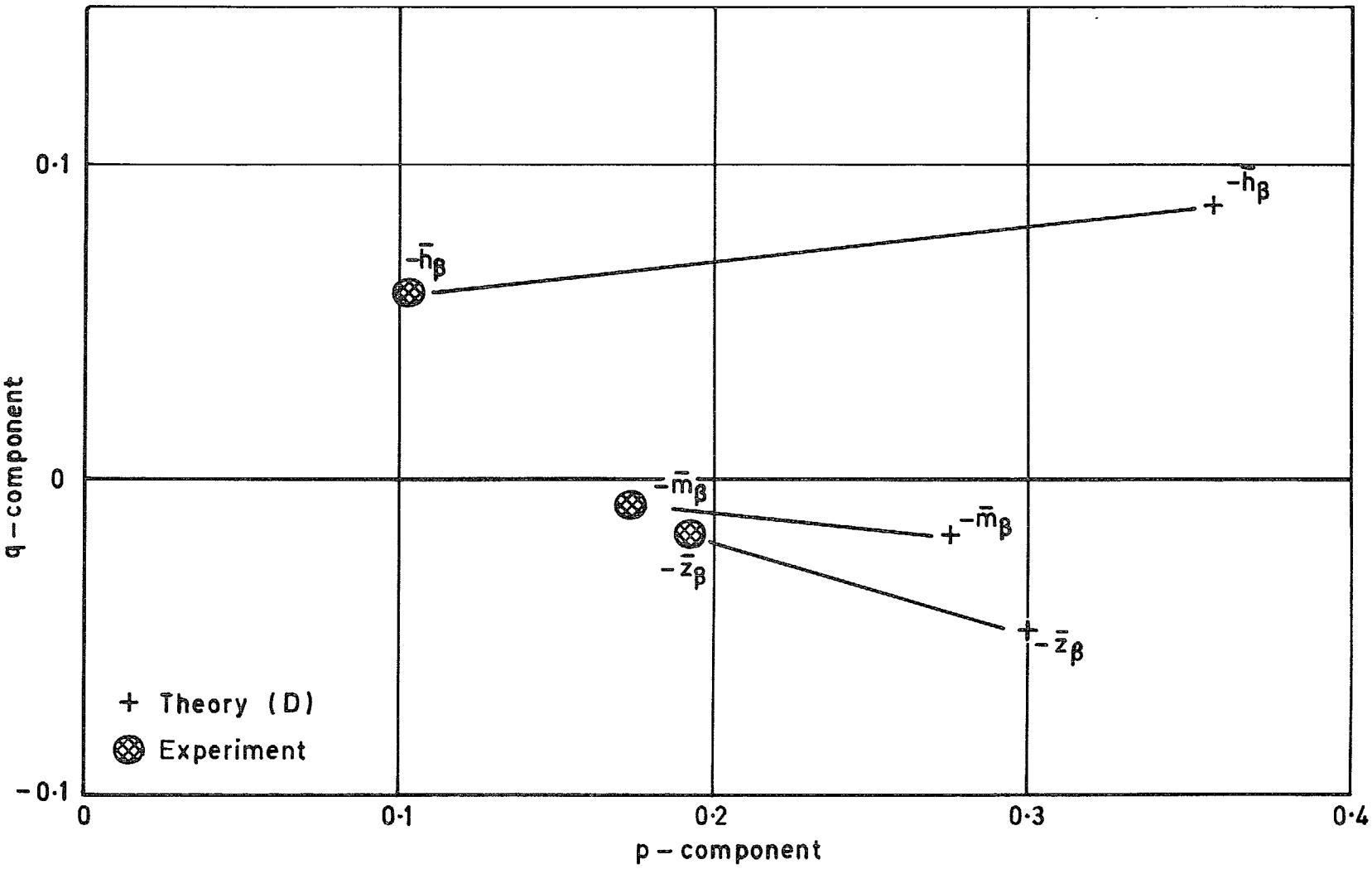

FIG. 28. Comparison of theory and experiment. Complex derivatives for $M = 0{\cdot}927$, $\bar{\nu} = 0{\cdot}27$.

First published 1977

HER MAJESTY'S STATIONERY OFFICE

Government Bookshops

49 High Holborn, London WC1V 6HB
13a Castle Street, Edinburgh EH2 3AR
41 The Hayes, Cardiff CF1 1JW
Brazennose Street, Manchester M60 8AS
Southey House, Wine Street, Bristol BS1 2BQ
258 Broad Street, Birmingham B1 2HE
80 Chichester Street, Belfast BT1 4JY

Government Publications are also available through booksellers

R. & M. No. 3806

ISBN 0 11 470977 7